doi.org/10.26434/chemrxiv.11786448.v1

DNA Inspirited Rational Construction of Nonconventional Luminophores with Efficient and Color-Tunable Afterglow

Yunzhong Wang, Saixing Tang, Yating Wen, Shuyuan Zheng, Bing Yang, Wang Zhang Yuan

Submitted date: 01/02/2020 • Posted date: 03/02/2020

Citation information: Wang, Yunzhong; Tang, Saixing; Wen, Yating; Zheng, Shuyuan; Yang, Bing; Yuan, Wang Zhang (2020): DNA Inspirited Rational Construction of Nonconventional Luminophores with Efficient and Color-Tunable Afterglow. ChemRxiv. Preprint. https://doi.org/10.26434/chemrxiv.11786448.v1

Persistent room-temperature phosphorescence (p-RTP) from pure organics is attractive due to its fundamental importance and potential applications in molecular imaging, sensing, encryption, anticounterfeiting, etc.1-4 Recently, efforts have been also made in obtaining color-tunable p-RTP in aromatic phosphors5 and nonconjugated polymers6,7. The origin of color-tunable p-RTP and the rational design of such luminogens, particularly those with explicit structure and molecular packing, remain challenging. Noteworthily, nonconventional luminophores without significant conjugations generally possess excitation-dependent photoluminescence (PL) because of the coexistence of diverse clustered chromophores6,8, which strongly implicates the possibility to achieve color-tunable p-RTP from their molecular crystals assisted by effective intermolecular interactions. Here, inspirited by the highly stable double-helix structure and multiple hydrogen bonds in DNA, we reported a series of nonconventional luminophores based on hydantoin (HA), which demonstrate excitation-dependent PL and color-tunable p-RTP from sky-blue to yellowish-green, accompanying unprecedentedly high PL and p-RTP efficiencies of up to 87.5% and 21.8%, respectively. Meanwhile, the p-RTP emissions are resistant to vigorous mechanical grinding, with lifetimes of up to 1.74 s. Such robust, color-tunable and highly efficient p-RTP render the luminophores promising for varying applications. These findings provide mechanism insights into the origin of color-tunable p-RTP, and surely advance the exploitation of efficient nonconventional luminophores.

File list (2)

DNA inspirited rational construction of nonconventional luminophores with efficient and color-tunable afterglow

Yunzhong Wang[1], Saixing Tang[1], Yating Wen[2], Shuyuan Zheng[1], Bing Yang[2] and Wang Zhang Yuan[1]*

[1]School of Chemistry and Chemical Engineering, Shanghai Key Lab of Electrical Insulation and Thermal Aging, Shanghai Electrochemical Energy Devices Research Center, Shanghai Jiao Tong University, Shanghai 200240, China.
[2]State Key Laboratory of Supramolecular Structure and Materials, College of Chemistry, Jilin University, Changchun 130012, China.
*e-mail: wzhyuan@sjtu.edu.cn

Keywords: nonconventional luminophores, persistent room temperature phosphorescence, color-tunable phosphorescence, clustering-triggered emission, through-space conjugation

Persistent room-temperature phosphorescence (p-RTP) from pure organics is attractive due to its fundamental importance and potential applications in molecular imaging, sensing, encryption, anticounterfeiting, etc.[1-4] Recently, efforts have been also made in obtaining color-tunable p-RTP in aromatic phosphors[5] and nonconjugated polymers[6,7]. The origin of color-tunable p-RTP and the rational design of such luminogens, particularly those with explicit structure and molecular packing, remain challenging. Noteworthily, nonconventional luminophores without significant conjugations generally possess excitation-dependent photoluminescence (PL) because of the coexistence of diverse clustered chromophores[6,8], which strongly implicates the possibility to achieve color-tunable p-RTP from their molecular crystals assisted by effective intermolecular interactions. Here, inspirited by the highly stable double-helix structure and multiple hydrogen bonds in DNA, we reported a series of nonconventional luminophores based on hydantoin (HA), which demonstrate excitation-dependent PL and color-tunable p-RTP from sky-blue to yellowish-green, accompanying unprecedentedly high PL and p-RTP efficiencies of up to 87.5% and 21.8%, respectively. Meanwhile, the p-RTP emissions are resistant to vigorous mechanical grinding, with lifetimes of up to 1.74 s. Such robust,

color-tunable and highly efficient p-RTP render the luminophores promising for varying applications. These findings provide mechanism insights into the origin of color-tunable p-RTP, and surely advance the exploitation of efficient nonconventional luminophores.

Persistent room temperature phosphorescence (p-RTP)[1-4,9-11] or long persistent luminescence (LPL) from pure organic compounds[12] are being extensively explored owing to the fundamental importance to unravel the dynamics of excitons in organics, and moreover for their applications in varying areas, such as watch indicator, molecular imaging[1,13,14], chemical sensors[15] and anticounterfeiting[16]. For the spin-forbidden nature of the intersystem crossing (ISC) process and high susceptibility of triplet excitons to molecular motions and quenchers in organic molecules[17], chemical and technical engineering endeavors were made to achieve p-RTP. In general, two main principles are followed: i) Introduction of heavy atoms[18] and/or heteroatoms[19] to enhance the spin-orbit coupling (SOC) and promote the consequent ISC processes; ii) Construction of rigid environments, such as crystal engineering[20,21], polymer matrix[22,23], H-aggregates[3,24], host-guest embedding[25] and organic-inorganic hybridation[26,27], to stabilize the triplet excitons. Among exciting advances in pure organic p-RTP, accessing color-tunable p-RTP represents one of the latest progress[5,6,28,29], which are promising in some significant areas like advanced anticounterfeiting and encoding. Rational design for such luminogens and the underlying mechanism for the tunability, however, remain elusive. For example, planar structure together with monomer and dimer phosphorescence[5], as well as diverse cluster emissions[6,28] were considered as the origin of tunable phosphorescence for different systems.

Recently, while we endeavored to the development of nonconventional luminophores free of classic large π-conjugates, it is found that concentrated solutions and/or solids of sodium alginate (SA)[30], polyacrylamide (PAM)[8] and bovine serum albumin (BSA)[6] exhibit variable cryogenic phosphorescence with different excitations. In particular, it has been demonstrated

that nonconventional luminophores generally show excitation-dependent photoluminescence (PL) at aggregated states, on account of the formation of varying clustered chromophores[31-33]. These results highly implicate the possibility to achieve tunable p-RTP from nonconventional luminophores, pending sufficiently stiffened conformations. Nevertheless, it remains an arduous task to access efficient nonconventional luminophores, particularly those with efficient and readily tunable p-RTP.

Here we use a group of pyrimidine molecules to demonstrate the rational design of such like nonconventional luminophores and moreover the origin of the tunability. It is well known that there are effective intra- and intermolecular interactions in biomolecules, which are highly important to stabilize specific structures and functions[34]. For example, four nucleobases, namely cytosine (C), guanine (G), adenine (A) and thymine (T), in the alternating sugar-phosphate backbone of DNA are bound together according to A-T and C-G base pairing rules, forming highly stable double helix with multiple hydrogen bonds (H-bonds, Fig. 1a)[35]. Such multiple H-bonds are also widely adopted in the supramolecular chemistry and self-healing materials[36], owing to their dynamic and robust characteristics. Inspirited by these noncovalent intermolecular interactions, hydantoin (HA) that resembles thymine in DNA, comes into our mind. As illustrated in Fig. 1b, multiple H-bonds could be expected in HA aggregates/crystals, which along with the cyclic planar structure would create rigid conformations; Furthermore, the presence of carbonyls (C=O) and nitrogen (N) heteroatoms would promote SOC and subsequent ISC process[37], thus beneficial to effectually generate triplet excitons. Meanwhile, the cyclic planar structure of HA may vanquish the problem of inefficient emission of nonconventional luminophores, considering Zhang et al. have exploited similar strategies to design highly efficient single benzene luminophores[38]. Owing to its overall short conjugation, individual HA molecules would be difficult to excite to offer remarkable emission. Their crystals, however, might exhibit tunable PL and RTP owing to the concurrence of diverse emissive species, promoted ISC and remarkably rigidified conformations (Fig. 1c). Taken

together, it seems highly probable to construct efficient nonconventional luminophores derived from HA with distinct RTP. Exactly, these luminophores exhibit outstanding PL efficiency (Φ) with an unprecedented record of 87.5%[31]. Furthermore, striking and tunable p-RTP with efficiency (Φ_p) and lifetime ($\langle\tau\rangle_p$) of up to 21.8% and 1.74 s was achieved, whose emission color readily changed from sky-blue to yellowish-green in response to the variation in excitation wavelength (λ_{ex}).

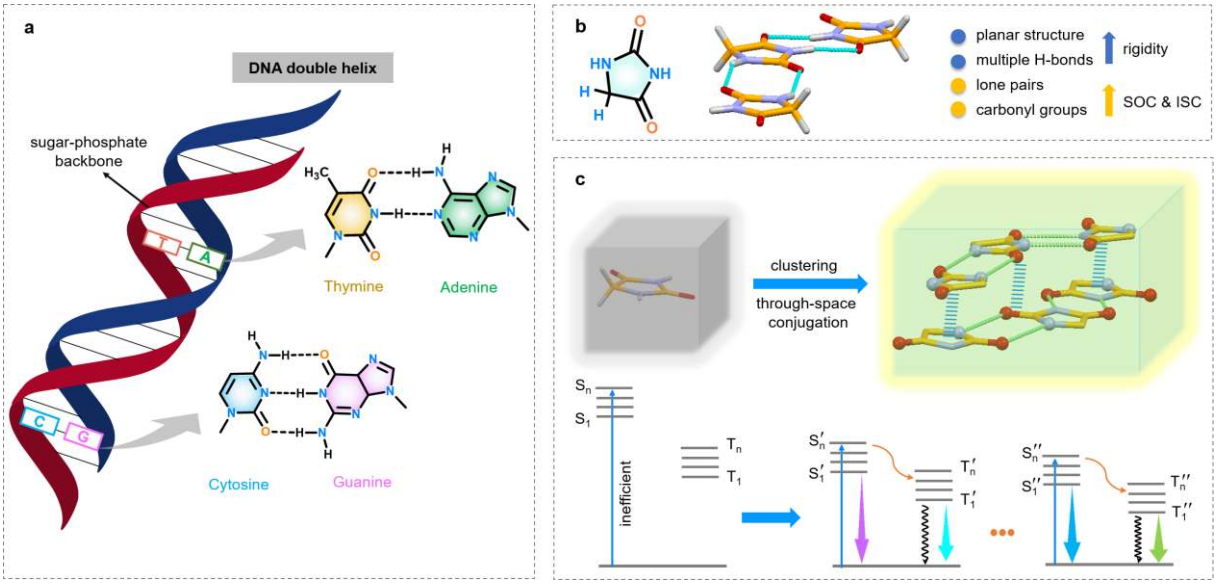

Fig. 1| Design rational for nonconventional luminogens with efficient and tunable p-RTP. **a**, Illustration of the DNA double helix. **b**, Structure, multiple H-bonds and inherent features of HA. **c**, Schematic illustration of individual (nonemissive) and clustered (emissive) HA molecules and their corresponding Jablonski diagrams for the generation of tunable emission. The structure features and clustered chromophores in crystals are the key design points for accessing efficient and tunable p-RTP in this work.

HA is commercially available and used after recrystallization. Its purity was verified by ^{1}H and ^{13}C NMR spectroscopies (Fig. S1 and S2) and single crystal crystallography (Table S1). HA is widely utilized in diverse areas like the synthesis of pharmaceutical intermediates, precusors of functional resins and antimicrobial agents[39]. However, so far, rare researches concern on its PL properties, presumably owing to the absence of classic chromophores and the consequent preconception of its nonluminescence[40]. Actually, according to the clustering-triggered emission (CTE) mechanism[41-43], HA is a promising luminophore, on account of its molecular p-π conjugation and effective intermolecular interactions in aggregates, which would

result in extend electron delocalization via the through-space conjugation accompanying conformation rigidification. Indeed, despite being almost nonluminescent in dilute solutions (i.e. 10^{-4} M), it gets emissive in concentrated solutions (≥ 0.05 M), and the PL intensity is gradually enhanced as the increase in concentration, featuring obvious concentration-enhanced emission characteristics (Fig. S9 and S10). Notably, various λ_{ex} values render changing emission peaks and shoulders at around 360/383/436/450/490/500 nm for 0.5 M solution (Fig. S9b and S11b), indicative of the presence of diverse emissive populations, which is further supported by their distinct lifetimes ($\langle\tau\rangle_f$) of 2.25, 9.11 and 9.70 ns at 360, 436 and 500 nm (Fig. S12a), respectively.

Above emission behaviors resemble most nonconventional luminophores and can well be rationalized by the CTE mechanism[41-43]. Namely, the clustering of HA molecules results in different emissive species with varying through space electronic delocalizations. These electronic interactions are also reflected by the absorption for concentrated solutions and crystals of HA, where enhanced absorption at ~300 nm and the tail in the visible region are found (Fig. S13). Additionally, concentrated solutions display λ_{ex}-dependent cryogenic (77 K) phosphorescence (Fig. S10). These results promoted us to further check the crystal emission, in the expectation of realizing tunable p-RTP. Fortunately, upon UV excitation, HA crystals exhibit bright blue emission (Fig. S14), and moreover, sky-blue and yellowish-green afterglows lasting for over 10 s are visualized after ceasing the 312 and 365 nm UV lights (Fig. 2a and Video S1). Further photophysical tests disclose changing PL peaks and shoulders for both prompt (351~476 nm) and delayed (433~539 nm) emissions with different λ_{ex}s for the crystals (Fig. 2b, S15 and S16). While most of the former can be ascribed to fluorescence, the latter is readily assignable to p-RTP. Subsequent time-resolved measurement reveals the long lifetimes of 1.54 and 1.74 s at 456 and 528 nm (Fig. 2c and Table S2), respectively, thus verifying their p-RTP nature. Notably, these $\langle\tau\rangle_p$ values are among the longest lifetimes recorded in pure

organics (Fig. S17)[2-5]. Meanwhile, the λ_{ex}-regulated p-RTP and their distinct lifetimes manifest they should essentially originate from disparate emissive clusters (Fig. 1c). Notably, the broad full-width at half-maximum (FWHM, > 82/154/97 nm) and multiple decay components of p-RTP (Fig. 2b and Table S2) further suggest the concurrence of heterogeneous emissive populations.

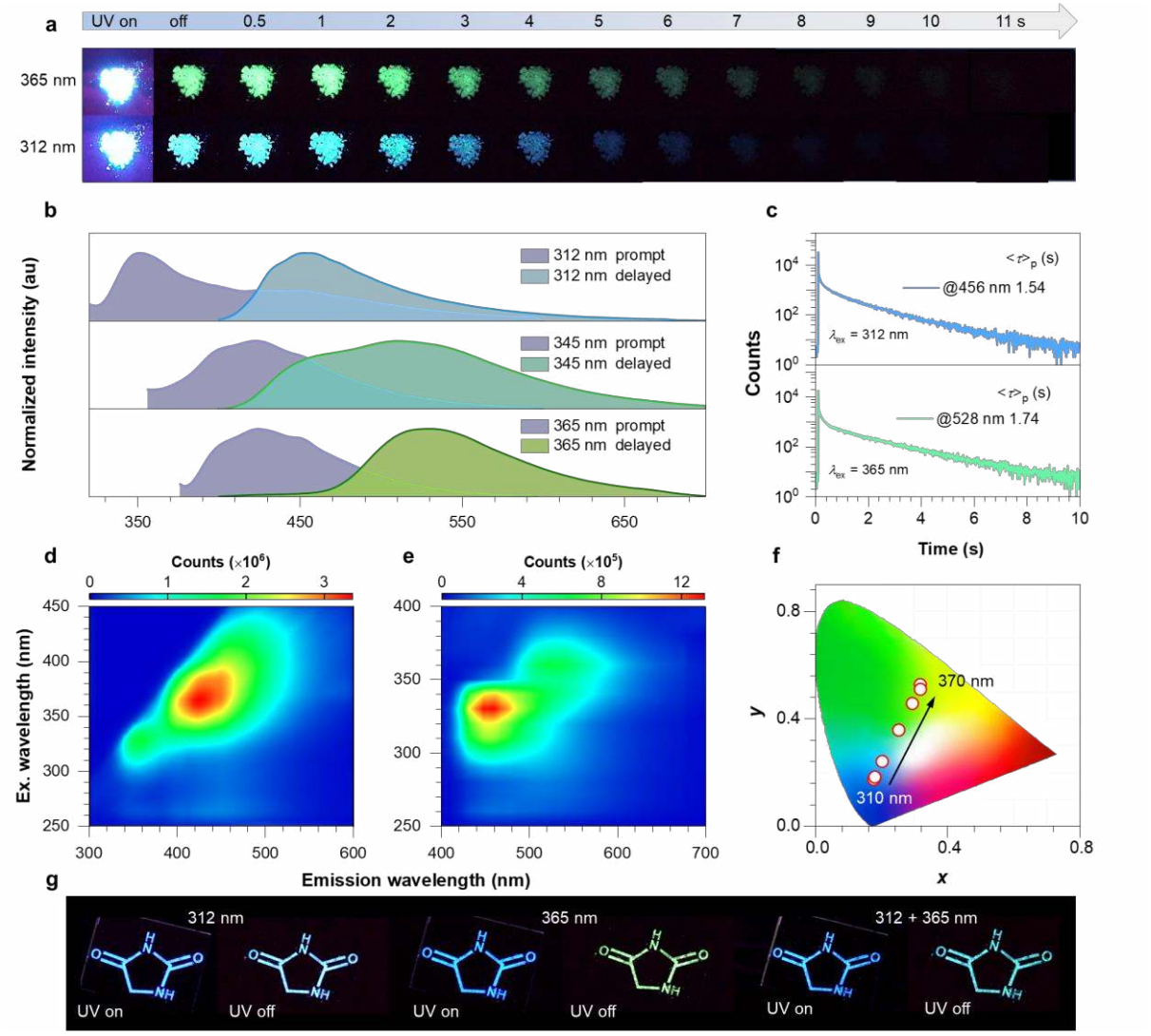

Fig. 2| Excitation-dependent PL and p-RTP of HA crystals. a, Photographs of HA crystals taken under 312 and 365 nm UV lights and after ceasing the UV irradiations. **b**, Prompt and delayed emission spectra of HA crystals under different λ_{ex}s. **c**, p-RTP lifetime profiles of HA crystals under excitations of 312 and 365 nm. **d**, Excitation-PL and **e**, excitation-p-RTP mappings of HA crystals at room temperature. **f**, The CIE coordinate diagram of p-RTP for HA crystals with changing λ_{ex}s. **g**, Demonstration of the advanced anticounterfeiting application based on the PL and color-tunable p-RTP of HA crystals.

Inspired by such an intriguing phenomenon, to further decipher the variation, excitation-PL and excitation-RTP mappings were recorded (Fig. 2d,e and S16). For the prompt PL, UV and/or

blue bands were/was noticed (Fig. S16). On account of the invisible nature of UV lights, though upon different irradiations, HA crystals glow similar blue lights (Fig. S14 and S18). For the p-RTP emission, variable peaks/shoulders in the blue and green regions are found when the λ_{ex} changes from 250 to 390 nm (Fig. 2b,d,e and S15). This tunable multicolor p-RTP is further confirmed by the CIE coordinate, which almost linearly changes from blue (0.18, 0.18) to yellowish-green (0.32, 0.51) with growing λ_{ex} (310~370 nm, Fig. 2f).

To quantitatively evaluate the emission of HA crystals, their efficiencies were determined, which are 5.3% and 87.5% with λ_{ex}s of 312 and 365 nm (Table S3), respectively. Combining their emission spectra, Φ_p values of 3.1% and 21.8% were correspondingly derived (Table S3). On one hand, these λ_{ex}-dependent efficiencies confirm anew the presence of different emissive species; on the other hand, such excellent Φ_p and long $\langle\tau\rangle_p$ (1.74 s) are amongst the best values for p-RTP emission from nonconventional luminophores[6-8,44], which are also exceeding those of most classic aromatic compounds (Fig. S17). These results unambiguously implicate the great potential of nonconventional luminophores, which could own comparable PL performances to those of classic luminogens. It is also noted that even being subjected to vigorous grinding, the ground powders also display bright PL and moreover p-RTP (Fig. S19), revealing their robust nature, which should stem from the powerful crystalline lattice (Fig. S19) and effective intermolecular interactions. Such robust, highly efficient and λ_{ex}-dependent p-RTP making them ready for diverse applications like encryption, anticounterfeiting, molecular imaging and UV detection without troublesome fabrication[4]. As exampled in Fig. 2g, the patterns of HA structure glow similar blue lights under varying λ_{ex}s, their afterglows, however, show distinctive blue (312 nm), cyan (312+365 nm) and green (365 nm) colors after the stop of UV lights, which render them outstanding candidates as advanced dynamic and multi-dimensional (luminescence, p-RTP, tunable afterglow) anticounterfeiting materials.

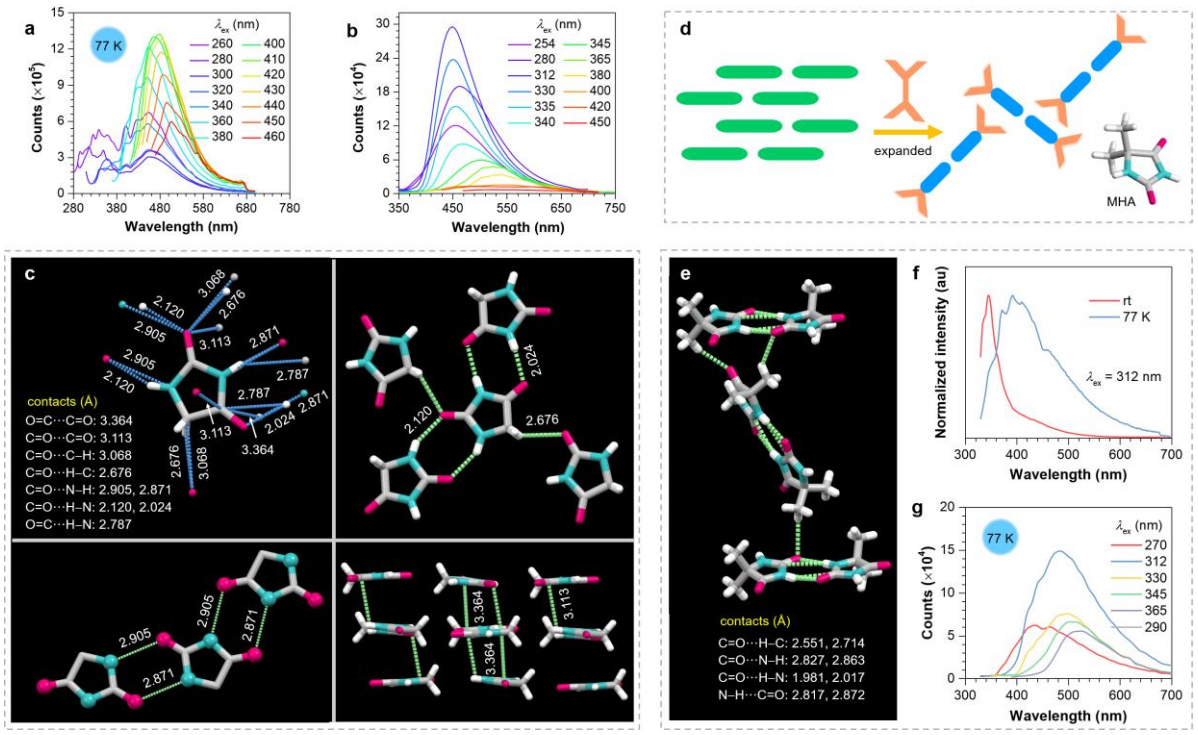

Fig. 3| Cryogenic emission, crystal structure and molecular packing of HA and MHA crystals. a,**b**, Emission spectra of HA crystals at varying λ_{ex}s with t_d of (**a**) 0 and (**b**) 0.1 ms. **c**, Structure, intermolecular interactions and fragmental packing of HA in crystals. **d**, Demonstration of the modulation of molecular packing through incorporation of steric hindrance. **e**, Structure and fragmental packing of MHA in crystals. **f**, PL spectra of MHA crystals at room temperature and 77 K with λ_{ex} of 312 nm. **g**, Delayed emission spectra (t_d = 0.1 ms) of MHA crystals at 77 K with varying λ_{ex}s.

To gain more insights, crystal emission at 77 K was further monitored. As depicted in Fig. 3a and S20, finely structured PL spectra with extension into both much bluer and redder regions were recorded at 77 K, while maintaining the λ_{ex}-dependence. With a delay time (t_d) of 0.1 ms, tunable phosphorescence with varying maximum in response to λ_{ex} is clearly identified (Fig. 3b). These cryogenic results again verify the coexistence of multiple emissive populations, and moreover suggest another possibility as the origin of the p-RTP tunability, which is distinct from the supposed case of monomer and dimer phosphorescence in planar TMOT system[5]. To further figure out the luminescence mechanism, single crystal structure of HA was examined. As shown in Fig. 3c, individual HA molecules adopt a planar conformation around with effective intermolecular interactions including expected multiple H-bonds (C=O···H–N, 2.024, 2.120 Å), C–H···O=C (2.676 Å), C=O···O=C (3.113 Å), N···O (2.871, 2.905 Å) and

O=C···C=O (π-π, 3.346 Å) short contacts, which synergistically retard molecular motions. Specifically, a notable supramolecular network is formed that adjacent molecules are almost extended in the very plane (Fig. 3c and S21). Furthermore, short distances among C=O groups in different layers empower strong π···π interactions, which would generate highly extended through-space delocalization. Therefore, though the limited conjugation of individual HA molecules cannot allow efficient excitation and emission, clustered molecules in an extended plane together with effective π···π interactions can offer vast electronic communication, thus leading to diverse emissive clusters with extended delocalization that responsible for λ_{ex}-dependent PL and p-RTP emissions (Fig. 1c).

To identify the effect of different electronic interactions on the tunability of phosphorescence, 5,5-dimethylhydantoin (MHA) was further investigated (Fig. S3 and S4), for which the intermolecular face to face π···π stacking might be significantly weakened owing to the incorporation of steric methyl groups (Fig. 3d). As expected, while multiple H-bonds retain in the MHA crystals, no strong π···π interactions are noticed (Fig. 3e and S22). With comparison to that of HA crystals, the emission of MHA crystals becomes weak and is hypsochromically shifted (i.e. 345 nm, λ_{ex} = 312 nm, Fig. 3f and S23a) at ambient conditions, owing to the decreased intermolecular interactions and electronic delocalizations. Such hypsochromic shift excludes the possibility of monomer emission at 356 nm for HA crystals, considering the same molecular conjugated skeleton of HA and MHA. In addition, even no noticeable visible PL is observed at room temperature, due to the disruption of effective electronic interactions and active vibrational dissipations. Upon cooling to 77 K, the PL is significantly enhanced (Fig. 3f and S24a); Furthermore, strikingly λ_{ex}-tunable phosphorescence is noticed (Fig. 3g and S24b). These results indicate that the tunability of phosphorescence does not rely on the specific aggregation, and it can well be understood in terms of the CTE mechanism[30,41,42]. Namely, the formation of diverse clustered chromophores is responsible for the tunable phosphorescence.

To further check the origin of tunable p-RTP and decode the effects of molecular conformation and packing on PL behaviors, especially on p-RTP emission and its tunability, we synthesized two dimeric derivatives of HA, namely 1,1'-methylenedihydantoin (MDHA) and 1,1'-(ethane-1,1-diyl)dihydantoin (EDHA) (Fig. S5-S8), through the facile condensation under acid conditions (Fig. 4a). Methyl and ethyl groups are adopted as linkers to afford different steric hindrance and thus generally distorted conformations with distinctive molecular packings. Indeed, both MDHA and EDHA adopt highly distorted conformations in crystals, accompanying effective intermolecular interactions (Fig 4b, S25 and S26) and intramolecular through-space conjugations (Fig. 4a and S27). Moreover, despite without π-π stacking, such intermolecular interactions as C=O···N and C=O···C=O among the subgroups bearing π and *n* electrons are apparently observed (Fig. 4b and S26), which are ready to generate diverse clustered chromophores with varying electronic delocalizations.

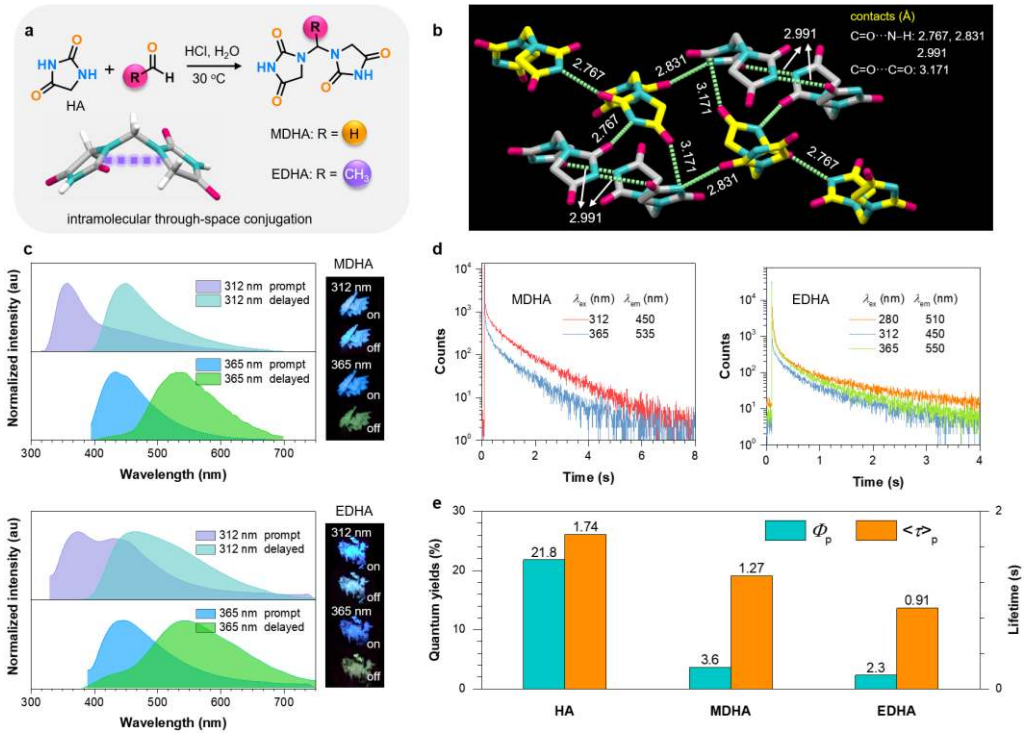

Fig. 4| Excitation-dependent PL and p-RTP of MDHA and EDHA crystals. a, Synthetic route to MDHA and EDHA with intramolecular through-space conjugation. **b**, Crystal structure and fragmental molecular packing with denoted through-space conjugation for MDHA. **c**, Prompt and delayed emission spectra of MDHA and EDHA crystals under 312 and 365 nm excitation. Insets: photographs of MDHA and EDHA crystals taken under 312 and 365 nm UV lights or after ceasing the irradiations. **d**, Time-resolved decay profiles of MDHA and EDHA crystals monitored at different wavelengths. **e**, Φ_p and $\langle\tau\rangle_p$ for HA, MDHA and EDHA crystals.

Both crystals demonstrate resembling emission behaviors to those of HA crystals, accompanying with λ_{ex}-tunable PL and p-RTP (Fig. 4c, S28-S30). Upon 312 and 365 nm UV irradiations, MDHA and EDHA crystals both own analogous blue PL; however, they exhibit distinct p-RTP after ceasing the excitations, with emission colors of sky-blue and yellowish-green (Fig. 4c and S29), respectively. With λ_{ex} being changed from 312 to 365 nm, the main peaks of p-RTP shift from 450, 465 nm to 535, 550 nm for MDHA and EDHA crystals (Fig. 4c), respectively. Notably, upon excitation by 280 nm UV light, EDHA crystals show another p-RTP maximum at 510 nm (Fig. S30b), proving the presence of multiform emission species. Furthermore, the excitation-RTP mapping and corresponding CIE coordinates of both crystals clearly illustrate their λ_{ex}-dependent features (Fig. S29), thus unambiguously testifying the tunability. $<\tau>_p$s of the crystals monitored at different emission wavelengths (λ_{em}s) varied from 0.67 to 1.27 s (Fig. 4d and Table S2), which are slightly lower than those for HA crystals. Meanwhile, Φ_ps of MDHA and EDHA crystals are significantly decreased to 3.6% and 2.3% (Fig. 4e and Table S3), respectively, which might be ascribed to the destruction of electronic interactions and activation of molecular motions. For instance, long-range planar alignments of MDHA molecules have been destructed, while H-bonds and other short contacts among HA rings are partially reserved (Fig. 4b), thus resulting in imperfect electronic delocalizations and weaker intra/intermolecular interactions. These effects collectively lead to more active nonradiative deactivations and consequently lower efficiencies. Notably, additional methyl brings about the steric hindrance effect. As a result, two HA rings in EDHA are more heavily twisted, which limits the electronic communications and moreover increases the molecular motions, thus endowing it with the lowest Φ_p.

In conclusion, inspirited by the ubiquitous multiple H-bonds in DNA, nonaromatic HA, whose structure resembles that of thymine, was investigated. Thanks to the presence of C=O and N heteroatoms, effective through-space electronic delocalization, planar structure and abundant intermolecular interactions, HA is intrinsically highly luminescent with

unprecedented efficiencies of up to 87.5% in crystals, along with intriguing λ_{ex}-tunable multicolor p-RTP. Such p-RTP owns recorded Φ_p of 21.8% for nonconventional luminophores and long-lasting $\langle\tau\rangle_p$ of up to 1.74 s, which are amongst the best values even being compared with those of aromatics, as a result of significantly promoted SOC and consequently ISC transitions and immensely rigidified conformations.

Such fascinating tunability of p-RTP can well be rationalized in terms of the CTE mechanism. The presence of assorted emissive species with diverse electronic conjugation results in the λ_{ex}-dependent PL and p-RTP. Control experiments of MHA clearly indicate that specific aggregation (i.e. H-aggregation or π-π stacking) is not a necessity for accessing tunable afterglows, as it is readily observable at 77 K without such packing modes. Dimeric MDHA and EDHA with highly distorted conformations and intramolecular through-space conjugation also demonstrate excitation-regulating p-RTP, which also stems from the electronic communications among the moieties with π and *n* electrons alongside with conformation rigidification. These results unveil the universality of color-tunable afterglow in diverse compounds, regardless of their conformations or aggregation types.

In virtue of powerful supramolecular interactions, the p-RTP emission of HA crystals retains even upon vigorous mechanical grinding at ambient conditions. Such robust, color-tunable and efficient p-RTP endow the crystals extensively applicable in advanced anticounterfeiting, encryption and molecular imaging without troublesome fabrication processes. This work provides a new approach towards efficient nonconventional luminophores through powerful supramolecular interactions and effective electronic communications, and moreover shed new lights on the origination of tunability for organic afterglows.

Acknowledgements

This work was supported by the National Nature Science Foundation of China (51822303 and 51473092).

Author contributions

Y. Wang and W.Z.Y. conceived the project and experiments. Y. Wang finished the data acquisition and composed the draft manuscript. S.T. contributed to the measurement of PL spectra of HA solutions and the synthesis of EDHA. All authors contributed to the data analysis. W.Z.Y. supervised the whole project and thoroughly revised the manuscript.

Competing interests

The authors declare no competing interests.

Additional information

Supplementary information is available for this paper.

Methods

^{1}H and ^{13}C NMR spectra were recorded on a Bruker DRX 500 NMR spectrometer (Germany) using deuterated dimethyl sulfoxide (DMSO-d_6) as solvent at room temperature. The prompt photoluminescence (PL) spectra, excitation-PL mappings, excitation-phosphorescence mappings (t_d = 0.1 ms) and phosphorescence lifetimes ($\langle\tau\rangle_p$) for solids were all measured on an Edinburgh FLS1000 photoluminescence spectrometer. The prompt PL spectra of solutions were measured on a Perkin-Elmer LS 55 PL spectrometer. Absorption spectra of crystals and solutions were measured on PerkinElmer Lambda750s and Lambda 35 UV/Vis spectrometer, respectively. Fluorescence lifetimes ($\langle\tau\rangle_f$) of the samples were measured on QM/TM/IM steady-state & time-resolved fluorescence spectrofluorometer (PTI, USA). The absolute quantum efficiencies (Φ) were measured with an Absolute PL Quantum Yield Spectrometer Quantaurus-QY C11347-11. The single crystal structure determination was performed on a Bruker D8 VENTURE X-ray Diffractometer at room temperature. All photographs and videos

were taken by a digital camera (Sony α7s II , Japan). Freeze-drying was performed on a FD-2D freeze dryer (Bilang Instrument Co., Ltd, Shanghai).

Received: xxxxx
Revised: xxxxxx
Published online: xxxxxx

References

1. Zhang, G.; Palmer, G. M.; Dewhirst, M. W.; Fraser, C. L. A Dual-Emissive-Materials Design Concept Enables Tumour Hypoxia Imaging. *Nat. Mater.* **2009**, *8*, 747–751.
2. Hirata, S.; Totani, K.; Zhang, J.; Yamashita, T.; Kaji, H.; Marder, S. R.; Watanabe, T.; Adachi, C. Efficient Persistent Room Temperature Phosphorescence in Organic Amorphous Materials under Ambient Conditions. *Adv. Funct. Mater.* **2013**, *23*, 3386–3397.
3. An, Z.; Zheng, C.; Tao, Y.; Chen, R.; Shi, H.; Chen, T.; Wang, Z.; Li, H.; Deng, R.; Liu, X.; Huang, W. Stabilizing Triplet Excited States for Ultralong Organic Phosphorescence. *Nat. Mater.* **2015,** *14*, 685–690.
4. He, Z.; Gao, H.; Zhang, S.; Zheng, S.; Wang, Y.; Zhao, Z.; Ding, D.; Yang, B.; Zhang, Y.; Yuan, W. Z. Achieving Persistent, Efficient, and Robust Room-Temperature Phosphorescence from Pure Organics for Versatile Applications. *Adv. Mater.* **2019**, *31*, 1807222.
5. Gu, L.; Shi, H.; Bian, L.; Gu, M.; Ling, K.; Wang, X.; Ma, H.; Cai, S.; Ning, W.; Fu, L.; Wang, H.; Wang, S.; Gao, Y.; Yao, W.; Huo, F.; Tao, Y.; An, Z.; Liu, X.; Huang, W. Colour-Tunable Ultra-Long Organic Phosphorescence of A Single-Component Molecular Crystal. *Nat. Photonics* **2019**, *13*, 406–411.
6. Wang, Q.; Dou, X.; Chen, X.; Zhao, Z.; Wang, S.; Wang, Y.; Sui, K.; Tan, Y.; Gong, Y.; Zhang, Y.; Yuan, W. Z. Reevaluating Protein Photoluminescence: Remarkable Visible Luminescence upon Concentration and Insight into the Emission Mechanism. *Angew. Chem. Int. Ed.* **2019**, *58*, 12667–12673.
7. Cai, S.; Ma, H.; Shi, H.; Wang, H.; Wang, X.; Xiao, L.; Ye, W.; Huang, K.; Cao, X.; Gan, N.; Ma, C.; Gu, M.; Song, L.; Xu, H.; Tao, Y.; Zhang, C,; Yao, W.; An, Z.; Huang, W. Enabling Long-Lived Organic Room Temperature Phosphorescence in Polymers by Subunit Interlocking. *Nat. Commun.* **2019**, *10*, 4247.
8. Zhou, Q.; Wang, Z.; Dou, X.; Wang, Y.; Liu, S.; Zhang, Y.; Yuan, W. Z. Emission Mechanism Understanding and Tunable Persistent Room Temperature Phosphorescence of Amorphous Nonaromatic Polymers. *Mater. Chem. Front.* **2019**, *3*, 257–264.
9. Zhao, W.; He, Z.; Lam, J. W. Y.; Peng, Q.; Ma, H.; Shuai, Z.; Bai, G.; Hao, J.; Tang, B. Z. Rational Molecular Design for Achieving Persistent and Efficient Pure Organic Room-Temperature Phosphorescence. *Chem* **2016**, *1*, 592–602.
10. Mao, Z.; Yang, Z.; Mu, Y.; Zhang, Y.; Wang, Y. F.; Chi, Z.; Lo, C. C.; Liu, S.; Lien, A.; Xu, J. Linearly Tunable Emission Colors Obtained from a Fluorescent-Phosphorescent Dual-Emission Compound by Mechanical Stimuli. *Angew. Chem. Int. Ed.* **2015,** *54*, 6270–6273.
11. Yang, J.; Zhen, X.; Wang, B.; Gao, X.; Ren, Z.; Wang, J.; Xie, Y.; Li, J.; Peng, Q.; Pu, K.; Li, Z. The Influence of the Molecular Packing on the Room Temperature Phosphorescence of Purely Organic Luminogens. *Nat. Commun.* **2018**, *9*, 840.
12. Kabe, R.; Adachi, C. Organic Long Persistent Luminescence. *Nature* **2017**, *550*, 384–387.

13. Fateminia, S. M. A.; Mao, Z.; Xu, S.; Yang, Z.; Chi, Z.; Liu, B. Organic Nanocrystals with Bright Red Persistent Room-Temperature Phosphorescence for Biological Applications. *Angew. Chem. Int. Ed.* **2017,** *56*, 12160–12164.
14. Pan, L.; Sun, S.; Zhang, A.; Jiang, K.; Zhang, L.; Dong, C.; Huang, Q.; Wu, A.; Lin, H. Truly Fluorescent Excitation-Dependent Carbon Dots and Their Applications in Multicolor Cellular Imaging and Multidimensional Sensing. *Adv. Mater.* **2015**, *27*, 7782–7787.
15. Zhou, Y.; Qin, W.; Du, C.; Gao, H.; Zhu, F.; Liang, G. Long-Lived Room-Temperature Phosphorescence for Visual and Quantitative Detection of Oxygen. *Angew. Chem. Int. Ed.* **2019**, *58*, 12102–12106.
16. Su, Y.; Phua, S. Z. F.; Li, Y.; Zhou, X.; Jana, D.; Liu, G.; Lim, W. Q.; Ong, W. K.; Yang, C.; Zhao, Y. Ultralong Room Temperature Phosphorescence from Amorphous Organic Materials toward Confidential Information Encryption and Decryption. *Sci. Adv.* **2018**, *4*, eaas9732.
17. Baryshnikov, G.; Minaev, B.; Agren, H. Theory and Calculation of the Phosphorescence Phenomenon. *Chem. Rev.* **2017,** *117*, 6500–6537.
18. Bolton, O.; Lee, K.; Kim, H. J.; Lin, K. Y.; Kim, J. Activating Efficient Phosphorescence from Purely Organic Materials by Crystal Design. *Nat. Chem.* **2011**, *3*, 205–210.
19. Baroncini, M.; Bergamini, G.; Ceroni, P., Rigidification or Interaction-Induced Phosphorescence of Organic Molecules. *Chem. Commun.* **2017**, *53*, 2081–2093.
20. Gong, Y.; Chen, G.; Peng, Q.; Yuan, W. Z.; Xie, Y.; Li, S.; Zhang, Y.; Tang, B. Z. Achieving Persistent Room Temperature Phosphorescence and Remarkable Mechanochromism from Pure Organic Luminogens. *Adv. Mater.* **2015**, *27*, 6195–6201.
21. He, Z.; Zhao, W.; Lam, J. W. Y.; Peng, Q.; Ma, H.; Liang, G.; Shuai, Z.; Tang, B. Z. White Light Emission from a Single Organic Molecule with Dual Phosphorescence at Room Temperature. *Nat. Commun.* **2017,** *8*, 416.
22. Reinekeand, S.; Baldo, M. A. Room Temperature Triplet State Spectroscopy of Organic Semiconductors. *Sci. Rep.* **2014**, *4*, 3797.
23. Ma, X.; Wang, J.; Tian, H. Assembling-Induced Emission: An Efficient Approach for Amorphous Metal-Free Organic Emitting Materials with Room-Temperature Phosphorescence *Acc. Chem. Res.* **2019**, *52*, 738–748.
24. Lucenti, E.; Forni, A.; Botta, C.; Carlucci, L.; Giannini, C.; Marinotto, D.; Pavanello, A.; Previtali, A.; Righetto, S.; Cariati, E. Cyclic Triim-idazole Derivatives: Intriguing Examples of Multiple Emissions and Ultralong Phosphorescence at Room Temperature. *Angew. Chem. Int. Ed.* **2017**, *56*, 16302–16307
25. Zhang, Z. Y.; Chen, Y.; Liu, Y. Efficient Room-Temperature Phosphorescence of a Solid-State Supramolecule Enhanced by Cu-curbit[6]uril. *Angew. Chem. Int. Ed.* **2019**, *131*, 6089–6093.
26. Zhou, B.; Yan, D. Hydrogen-Bonded Two-Component Ionic Crystals Showing Enhanced Long-Lived Room-Temperature Phosphorescence via TADF-Assisted Förster Resonance Energy Transfer. *Adv. Funct. Mater.* **2019**, *29*, 1807599.
27. Hu, H.; Meier, F.; Zhao, D.; Abe, Y.; Gao, Y.; Chen, B.; Salim, T.; Chia, E. E. M.; Qiao, X.; Deibel, C.; Lam, Y. M. Efficient Room-Temperature Phosphorescence from Organic-Inorganic Hybrid Perovskites by Molecular Engineering. *Adv. Mater.* **2018**, 1707621.
28. Chen, X.; Luo, W.; Ma, H.; Peng, Q.; Yuan, W. Z. Zhang, Y. Prevalent Intrinsic Emission from Nonaromatic Amino Acids and Poly(amino acids). *Sci. China Chem.* **2018**, *61*, 351–359.
29. Su, Y.; Zhang, Y.; Wang, Z.; Gao, W.; Jia, P.; Zhang, D.; Yang, C.; Li, Y.; Zhao, Y. Excitation-Dependent Long-Life Luminescent Polymeric Systems under Ambient Conditions. *Angew. Chem. Int. Ed.* 10.1002/anie.201912102.
30. Dou, X.; Zhou, Q.; Chen, X.; Tan, Y.; He, X.; Lu, P.; Sui, K.; Tang, B. Z.; Zhang, Y.; Yuan, W. Z. Clustering-Triggered Emission and Persistent Room Temperature Phosphorescence of Sodium Alginate. *Biomacromolecules* **2018**, *19*, 2014–2022.

31. Tomalia, D. A.; Klajnert-Maculewicz, B.; Johnson, K. A. M.; Brinkman, H. F.; Janaszewska, A.; Hedstrand, D. M. Non-Traditional Intrinsic Luminescence: Inexplicable Blue Fluorescence Observed for Dendrimers, Macromolecules and Small Molecular Structures Lacking Traditional/Conventional Luminophores. *Prog. Polym. Sci.* **2019**, *90*, 35–117.
32. Yuan, L.; Yan, H.; Bai, L; Bai, T.; Zhao, Y.; Wang, L.; Feng, Y. Unprecedented Multicolor Photoluminescence from Hyperbranched Poly(amino ester)s. *Macromol. Rapid Commun.* **2018**, *39*, 1800658.
33. Shang, C.; Wei, N.; Zhuo, H.; Shao, Y.; Zhang, Q.; Zhang, Z.; Wang, H. Highly Emissive Poly(maleic anhydride-alt-vinyl pyrrolidone) with Molecular Weight-Dependent and Excitation-Dependent Fluorescence. *J. Mater. Chem. C* **2017**, *5*, 8082–8090.
34. Kauzmann, W. Some Factors in the Interpretation of Protein Denaturation. Elsevier: **1959**, pp 1–63.
35. Donohue, J., Trueblood, K. N. Base pairing in DNA. *J. Mol. Biol.* **1960**, *2*, 363–371.
36. Yanagisawa, Y.; Nan, Y.; Okuro, K.; Aida, T. Mechanically Robust, Readily Repairable Polymers via Tailored Noncovalent Cross-Linking. *Science* **2018**, *359*, 72–76.
37. El-Sayed, M. A. Spin-Orbit Coupling and the Radiationless Processes in Nitrogen Heterocyclics. *J. Chem. Phys.* **1963,** *38*, 2834–2838.
38. Tang, B.; Wang, C.; Wang, Y.; Zhang, H. Efficient Red-Emissive Organic Crystals with Amplified Spontaneous Emissions Based on a Single Benzene Framework. *Angew. Chem. Int. Ed.* **2017,** *56*, 12543–12547.
39. Meusel, M.; Gütschow, M. Recent Developments in Hydantoin Chemistry. A Review. *Org. Prep. Proced. Int.* **2004**, *36*, 391–443.
40. Larson, D. B.; Arnett, J. F.; Seliskar, C. J.; McGlynn, S. P. Emissive Characteristics of Amidic Molecules. *J. Am. Chem. Soc.* **1974**, *96*, 3370–3380.
41. Gong, Y.; Tan, Y.; Mei, J.; Zhang, Y.; Yuan, W. Z.; Zhang, Y.; Sun, J.; Tang, B. Z. Room Temperature Phosphorescence from Natural Products: Crystallization Matters. *Sci. China Chem.* **2013**, *56*, 1178–1182.
42. Zhou, Q.; Cao, B.; Zhu, C.; Xu, S.; Gong, Y.; Yuan, W. Z.; Zhang, Y. Clustering-Triggered Emission of Nonconjugated Polyacrylonitrile. *Small* **2016**, *12*, 6586–6592.
43. Yuan, W. Z.; Zhang, Y. Nonconventional Macromolecular Luminogens with Aggregation-Induced Emission Characteristics. *J. Polym. Sci. Polym. Chem.* **2017**, *55*, 560–574.
44. Fang M.; Yang, J.; Xiang, X.; Xie, Y.; Dong, Y.; Peng, Q.; Li, Q.; Li, Z. Unexpected Room-Temperature Phosphorescence from A Non-aromatic, Low Molecular Weight, Pure Organic Molecule through the Intermolecular Hydrogen Bond. *Mater. Chem. Front.* **2018**, *2*, 2124–2129.

Supplementary Information

DNA inspirited rational construction of nonconventional luminophores with efficient and color-tunable afterglow

Yunzhong Wang[1], Saixing Tang[1], Yating Wen[2], Shuyuan Zheng[1], Bing Yang[2] and Wang Zhang Yuan[1]*

[1]School of Chemistry and Chemical Engineering, Shanghai Key Lab of Electrical Insulation and Thermal Aging, Shanghai Electrochemical Energy Devices Research Center, Shanghai Jiao Tong University, Shanghai 200240, China.
[2]State Key Laboratory of Supramolecular Structure and Materials, College of Chemistry, Jilin University, Changchun 130012, China.
*e-mail: wzhyuan@sjtu.edu.cn

Keywords: nonconventional luminophores, persistent room temperature phosphorescence, color-tunable phosphorescence, clustering-triggered emission, through-space conjugation

Experimental section

Materials. Hydantoin (HA) and 5,5-dimethylhydantoin (MHA) were purchased from Aladdin Reagent Co., Ltd. (Aladdin) and recrystallized before use. Formaldehyde (37 wt% in water) and hydrochloric acid (37 wt% in water) were bought from Sinopharm Chemical Reagent Co. Ltd. and used directly. Acetaldehyde (99.5%) was obtained from Aladdin Reagent Co., Ltd. (Aladdin) and used directly. Purified water was provided by Wahaha (Hangzhou) Co., Ltd.

General methods. ^{1}H and ^{13}C NMR spectra were recorded on a Bruker DRX 500 NMR spectrometer (Germany) using deuterated dimethyl sulfoxide (DMSO-d_6) as solvent at room temperature. The prompt photoluminescence (PL) spectra, excitation-PL mappings, excitation-phosphorescence mappings (t_d = 0.1 ms) and phosphorescence lifetimes ($\langle\tau\rangle_p$) for solids were all measured on an Edinburgh FLS1000 photoluminescence spectrometer. The prompt PL spectra of solutions were measured on a Perkin-Elmer LS 55 PL spectrometer. Absorption spectra of crystals

and solutions were measured on PerkinElmer Lambda750s and Lambda 35 UV/Vis spectrometer, respectively. Fluorescence lifetimes ($<\tau>_f$) of the samples were measured on QM/TM/IM steady-state & time-resolved fluorescence spectrofluorometer (PTI, USA). The absolute quantum efficiencies (Φ) were measured with an Absolute PL Quantum Yield Spectrometer Quantaurus-QY C11347-11. The single crystal structure determination was performed on a Bruker D8 VENTURE X-ray Diffractometer at room temperature. All photographs and videos were taken by a digital camera (Sony α7sⅡ, Japan). Freeze-drying was performed on a FD-2D freeze dryer (Bilang Instrument Co., Ltd, Shanghai).

Purification and synthesis. HA and MHA solids were first recrystallized and then were utilized for the cultivation of single crystals suitable for X-ray crystallography. MDHA and EDHA were synthesized according to Scheme S1. Their detailed synthesis and purification procedures are described below. **Note:** Samples utilized for measurements or for preparing the solutions are from the corresponding single crystals unless specified.

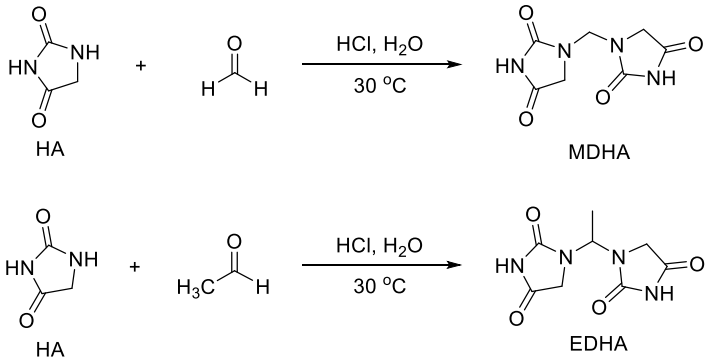

Scheme S1. Synthetic routes to MDHA and EDHA.

Purification of HA. Recrystallization of HA was performed through slow cooling its hot and saturated aqueous solution. The resulting crystals were collected through filtration and used for further cultivation of single crystals. Single crystals of HA suitable for X-ray crystallography were obtained by slow evaporation of its aqueous dilute solution at 25 °C. ^{1}H NMR (500 MHz, DMSO-

d_6) δ (ppm) 10.62 (s, 1H), 7.71 (s, 1H), 3.85 (d, J = 1.1 Hz, 2H). ^{13}C NMR (126 MHz, DMSO-d_6) δ (ppm) 174.33, 158.80, 47.69.

Purification of MHA. Recrystallization of MHA was performed through slow cooling its hot and saturated aqueous solution. Colorless crystals were obtained through filtration, and then were used for further cultivation of single crystals. Single crystals of MHA suitable for X-ray crystallography were obtained by slow evaporation of its aqueous dilute solution at 25 ºC. ^{1}H NMR (500 MHz, DMSO-d_6) δ (ppm) 10.55 (s, 1H), 7.94 (d, J = 3.8 Hz, 1H), 1.25 (s, 6H). ^{13}C NMR (126 MHz, DMSO-d_6) δ (ppm) 179.59, 156.39, 59.30, 25.07.

Synthesis of MDHA. HA powders (10.00 g, 0.1 mol) and purified water (10 mL) were placed into a single-necked flask. Then, concentrated hydrochloric acid (15 mL, 37 wt%) was slowly added under stirring. Afterwards, the flask was sealed with a rubber stopper, and aqueous solution of formaldehyde (5.2 mL, 37 wt%) was slowly injected with a syringe. The mixture was stirred at 30 °C for 72 h, and white paste-like solid-liquid mixture was obtained and then separated by suction filtration using a sand funnel. The obtained cake was washed with a large amount of purified water to obtain a white solid, which was freeze-dried for 3 days to yield a white solid powder (9.81 g). MDHA single crystals suitable for X-ray single crystal crystallography were obtained as colorless needle crystals by slow cooling of its hot aqueous solution. ^{1}H NMR (500 MHz, DMSO-d_6) δ (ppm) 10.87 (s, 2H), 4.74 (s, 2H), 3.94 (s, 4H). ^{13}C NMR (126 MHz, DMSO-d_6) δ (ppm) 172.19, 157.81, 50.49, 48.94.

Synthesis of EDHA. Following the similar procedure to that described above for MDHA, just changing the aqueous formaldehyde solution to acetaldehyde (4.24 mL, 0.08 mol), EDHA was obtained as white powders (8.72 g). MEHA single crystals suitable for X-ray single crystal crystallography were obtained as colorless needle crystals by slow cooling of its hot aqueous

solution. ^{1}H NMR (500 MHz, DMSO-d_6) δ (ppm) 10.82 (s, 2H), 5.68 (q, J = 6.9 Hz, 1H), 4.01 (d, J = 7.4 Hz, 4H), 1.45 (d, J = 7.0 Hz, 3H). ^{13}C NMR (126 MHz, DMSO-d_6) δ (ppm) 172.13, 156.60, 56.17, 48.71, 16.92.

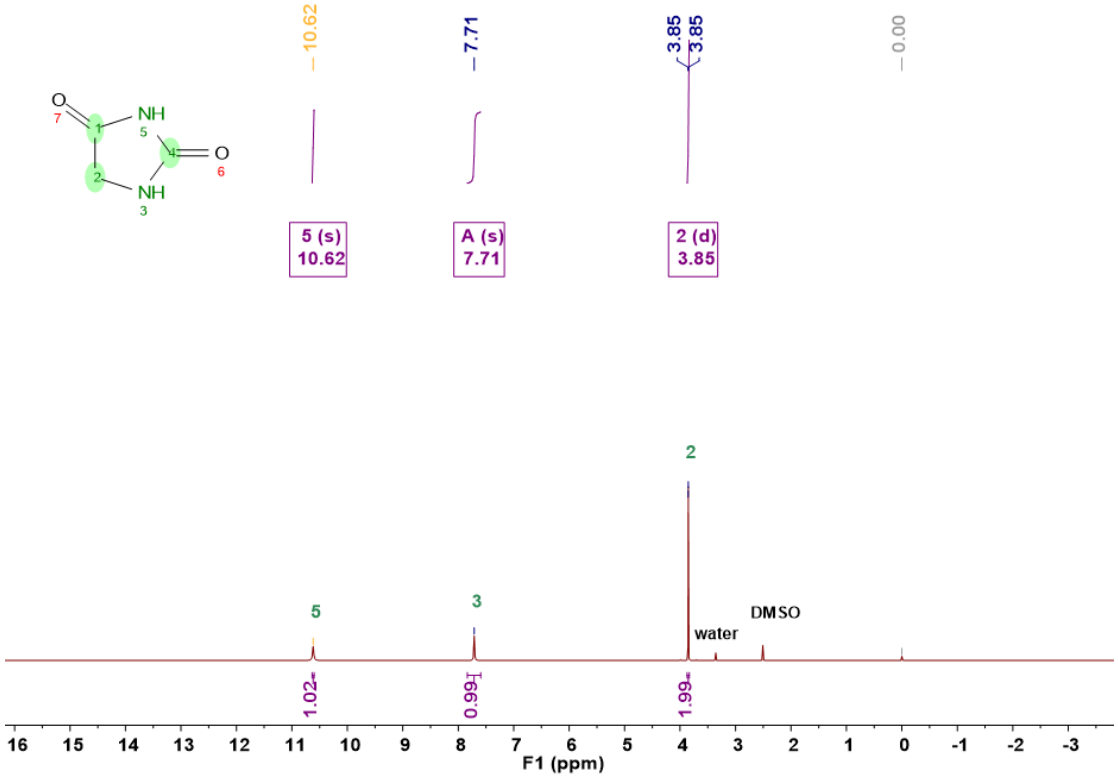

Fig. S1 ^{1}H NMR spectrum of HA in DMSO-d_6.

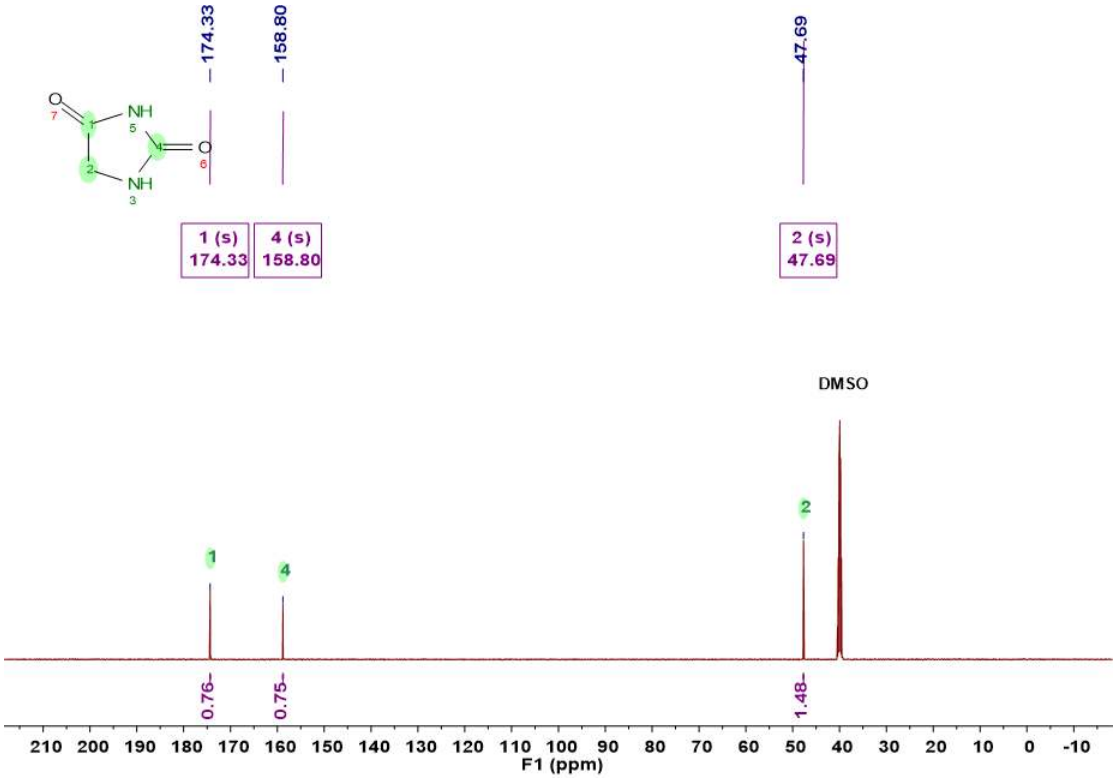

Fig. S2 ^{13}C NMR spectrum of HA in DMSO-d_6.

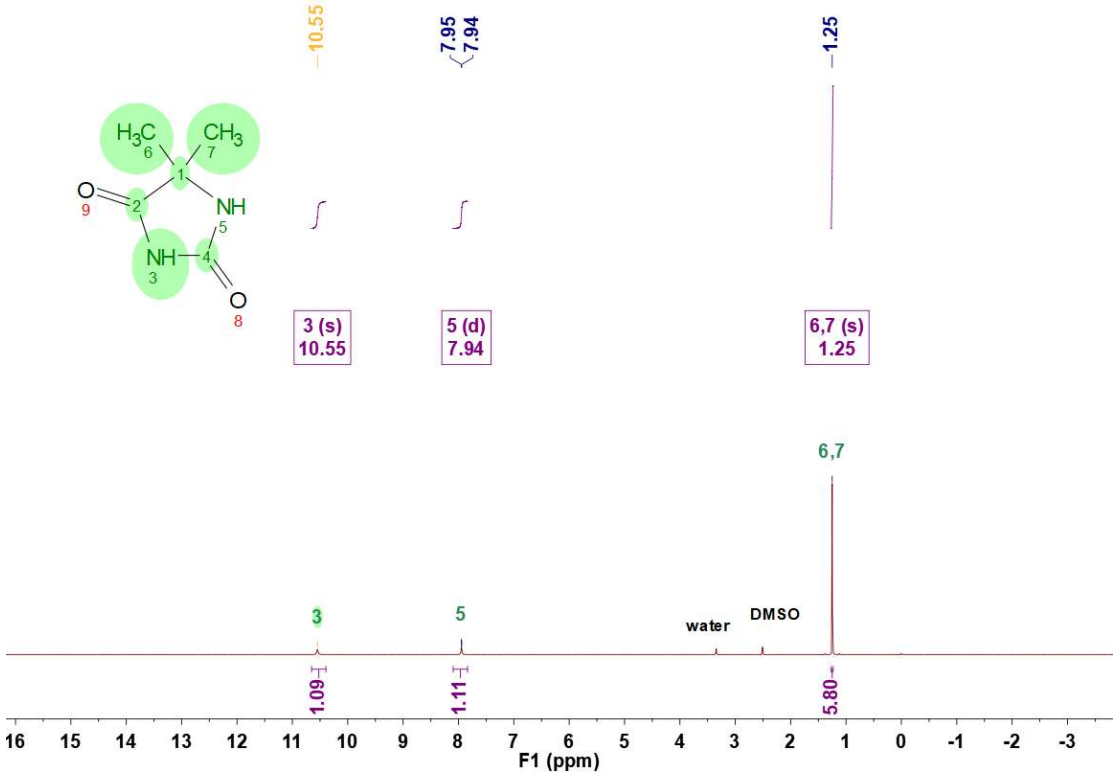

Fig. S3 ^{1}H NMR spectrum of MHA in DMSO-d_6.

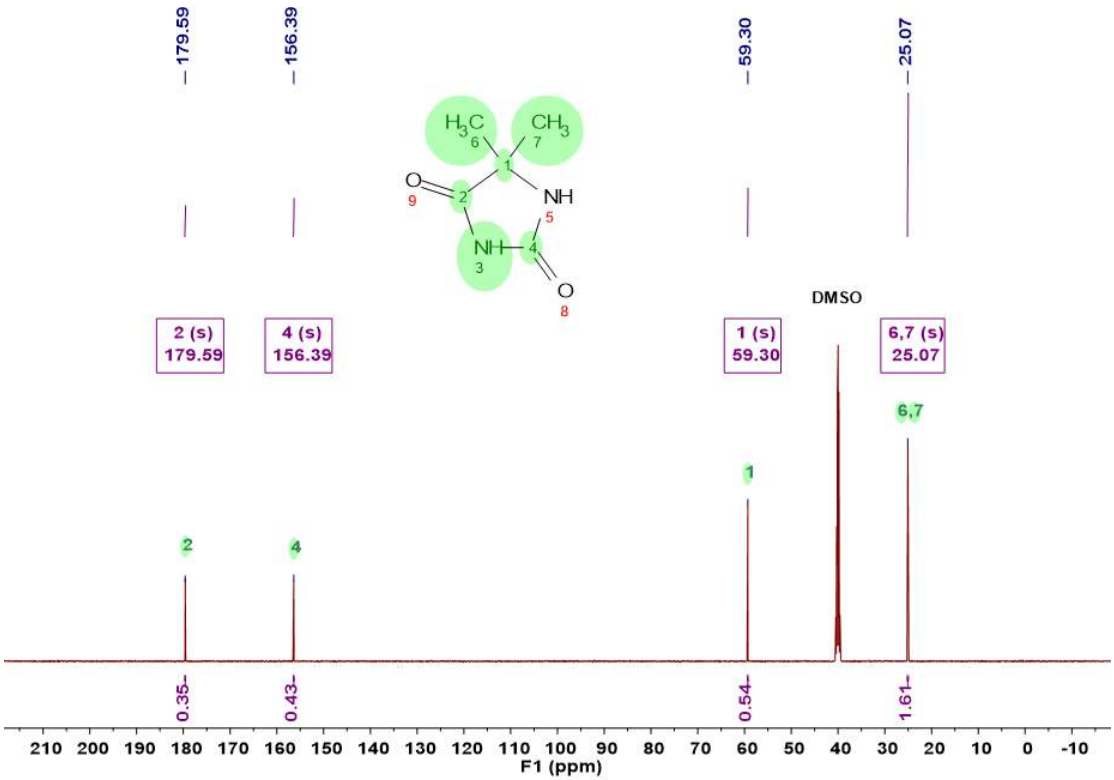

Fig. S4 ^{13}C NMR spectrum of MHA in DMSO-d_6.

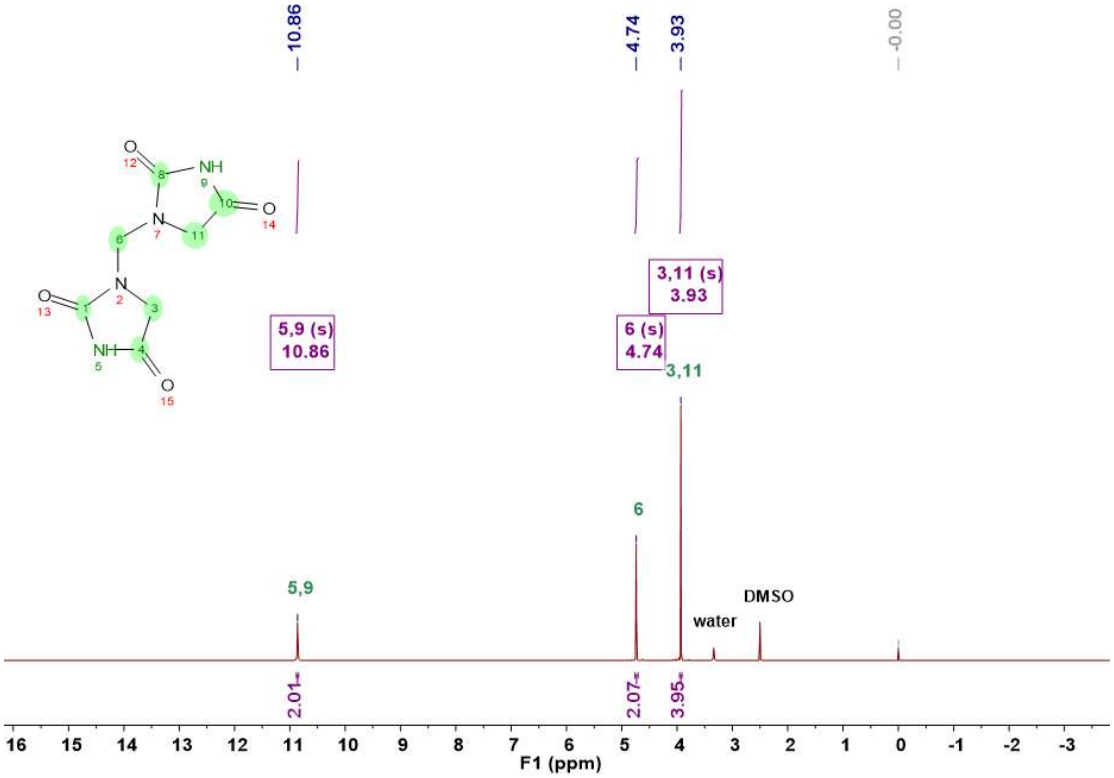

Fig. S5 ^{1}H NMR spectrum of MDHA in DMSO-d_6.

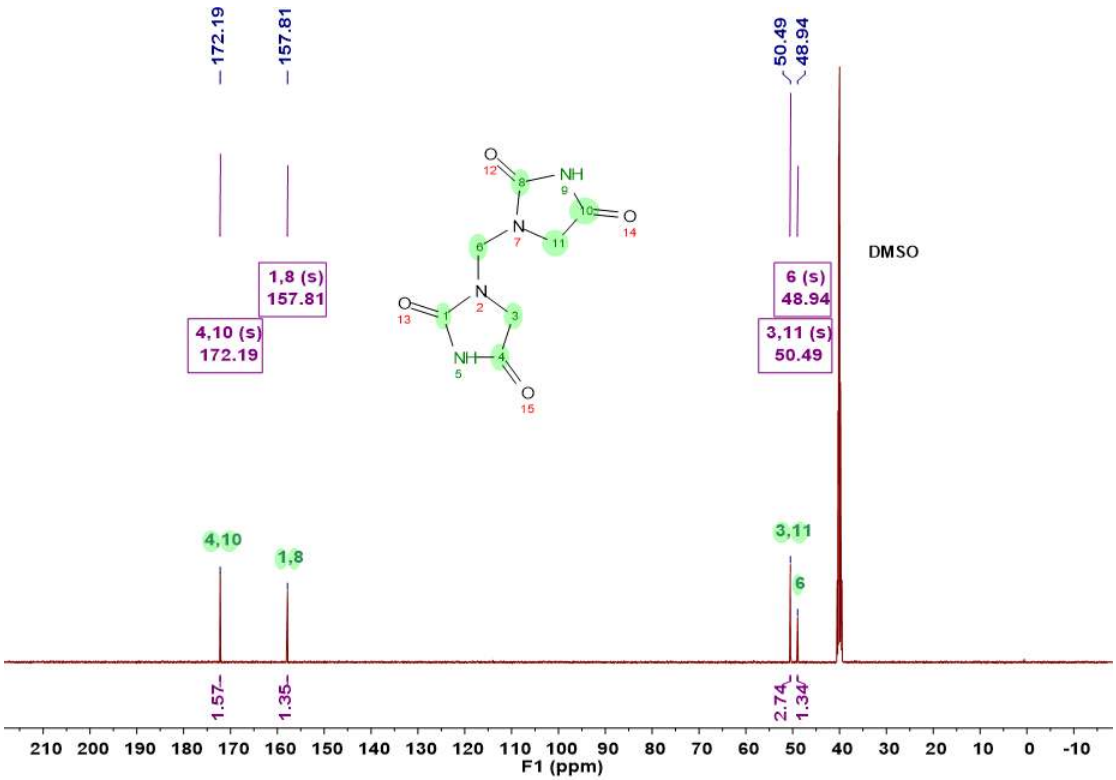

Fig. S6 ^{13}C NMR spectrum of MDHA in DMSO-d_6.

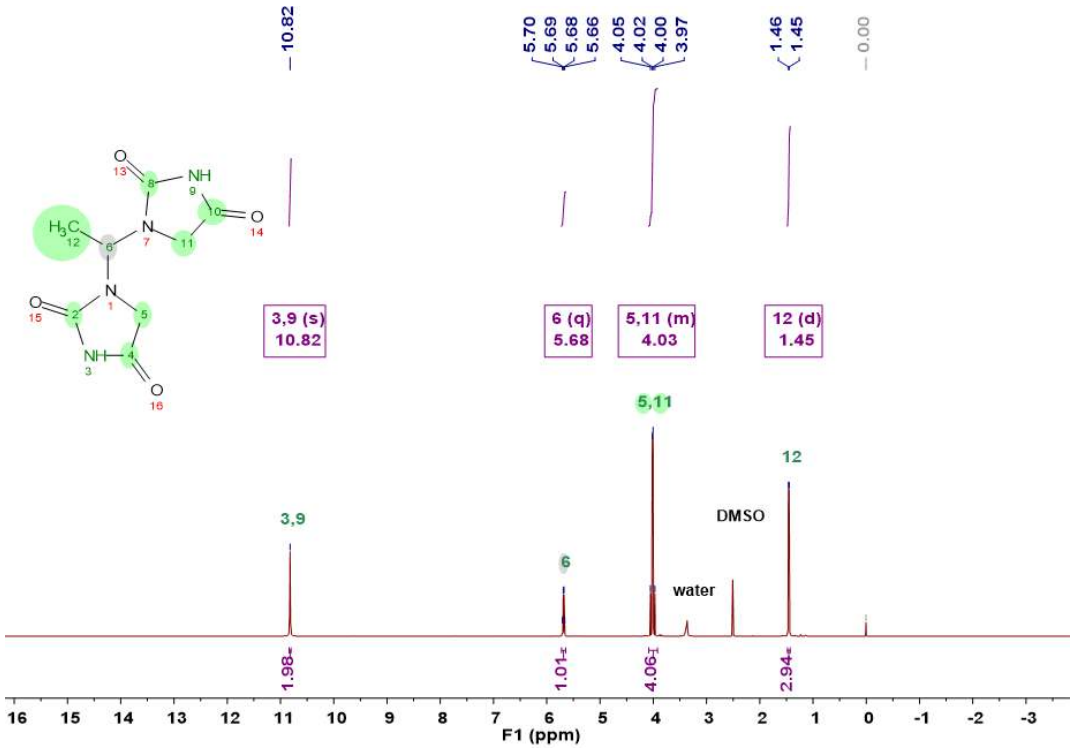

Fig. S7 ^{1}H NMR spectrum of EDHA in DMSO-d_6.

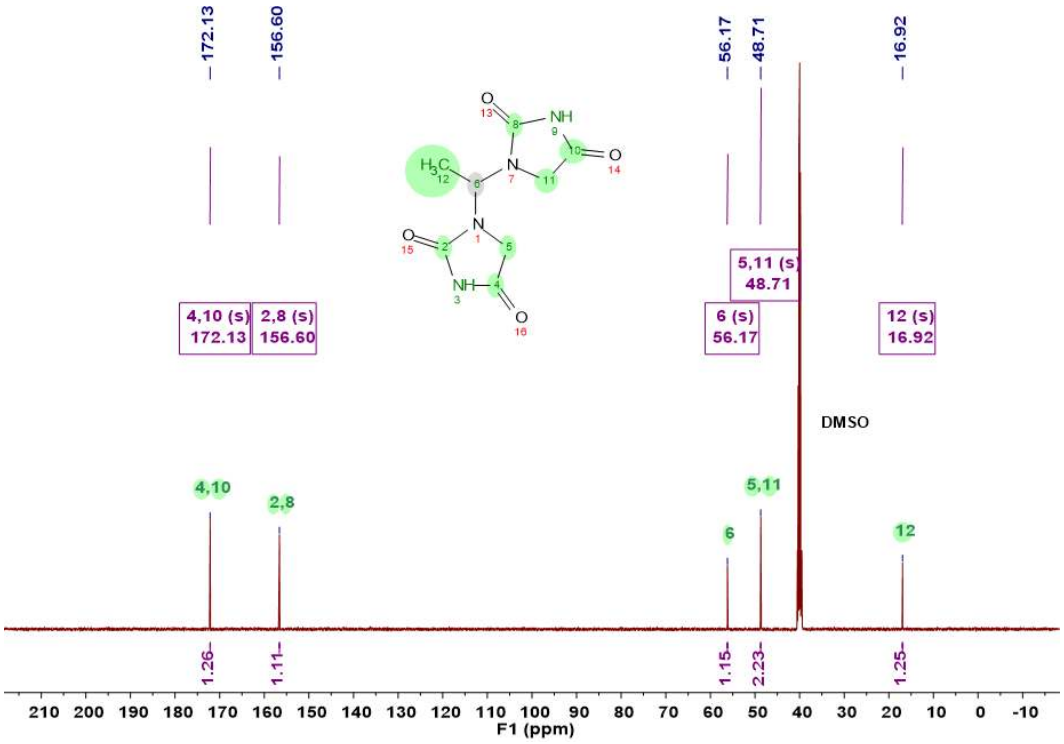

Fig. S8 ^{13}C NMR spectrum of EDHA in DMSO-d_6.

Table S1. Single crystal data of HA, MHA, MDHA and EDHA.

Name	Formula	Space Group	Cell Length [Å]	Cell Angle [°]	Cell Volume [Å^3]	Z	Density [g cm^{-3}]
HA	$C_3H_4N_2O_2$	Monoclinic, C2/c	a = 9.3446 (15) b = 12.244 (2) c = 7.3458 (13)	α = 90 β = 105.194 (7) γ = 90	811.1 (2)	8	1.639
MHA	$C_5H_8N_2O_2$	Orthorhombic, P2(1)2(1)2(1)	a = 7.1989 (6) b = 7.2267 (7) c = 13.0042 (13)	α = 90 β = 90 γ = 90	676.53 (11)	4	1.258
MDHA	$C_7H_8N_4O_4$	Monoclinic, P2(1)/n	a = 9.597 (3) b = 17.769 (5) c = 11.340 (4)	α = 90 β = 114.24 (4) γ = 90	1763.2 (11)	8	1.599
EDHA	$C_8H_{10}N_4O_4$	Monoclinic, P2(1)/c	a = 5.8982 (5) b = 12.4995 (11) c = 14.3372 (10)	α = 90 β = 114.292 (3) γ = 90	963.42 (14)	4	1.560

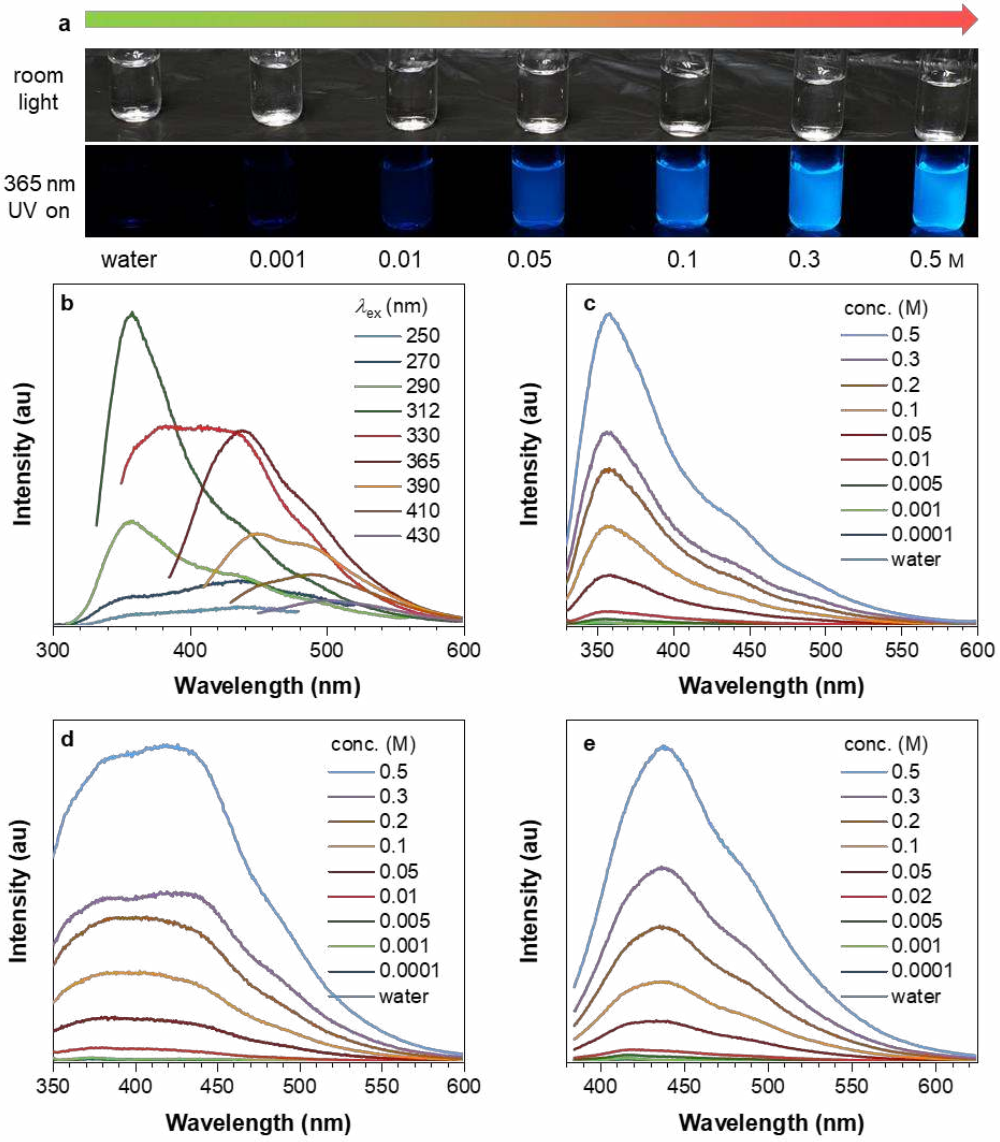

Fig. S9 a, Photographs of different aqueous solutions of HA under room light and 365 nm UV light. **b**, PL spectra of 0.5 M aqueous HA solution at different excitation wavelengths (λ_{ex}s). **c**–**e**, PL spectra of different aqueous solutions of HA with λ_{ex}s of (**c**) 312, (**d**) 330 and (**e**) 365 nm.

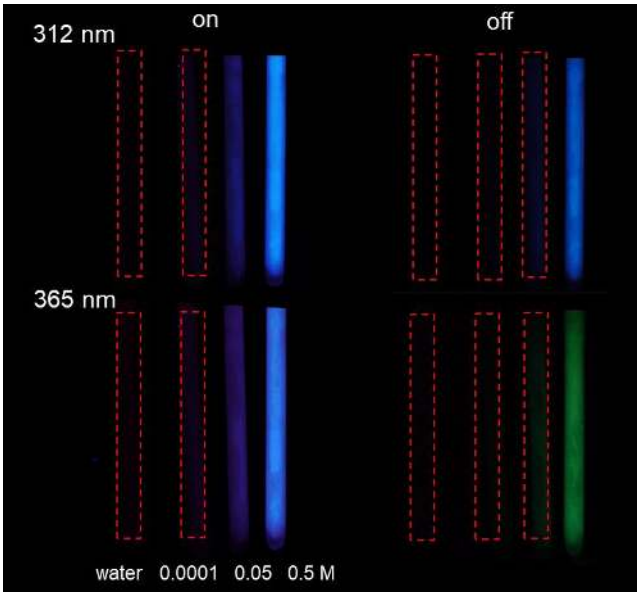

Fig. S10 Photographs of varying aqueous HA solutions taken before and after ceasing different UV excitations at 77 K.

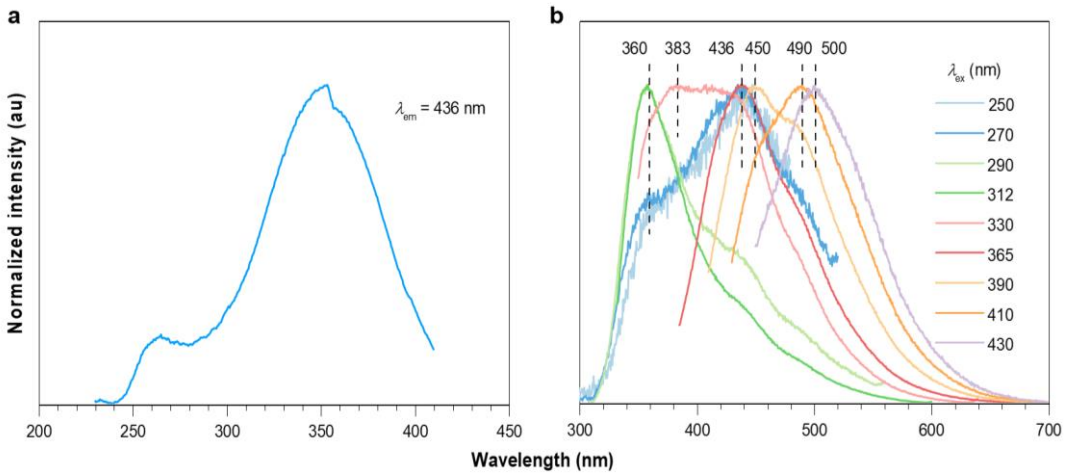

Fig. S11 a, Normalized excitation and **b**, emission spectra of 0.5 M aqueous HA solution.

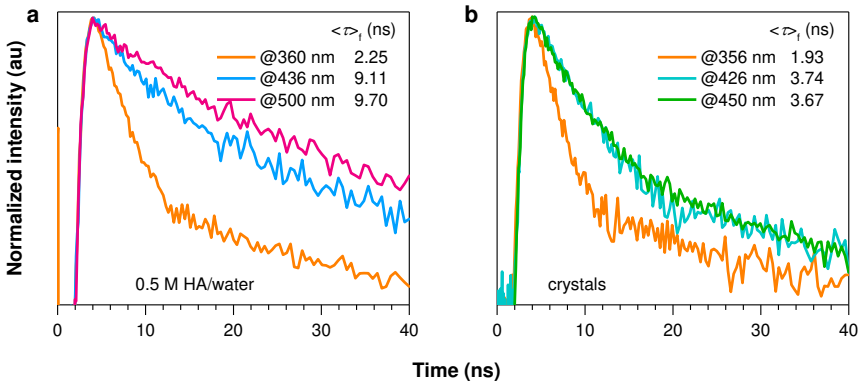

Fig. S12 a,**b**, Time-resolved decay profiles of fluorescence from (**a**) 0.5 M aqueous solution and (**b**) crystals of HA monitored at different wavelengths (λ_{ex} = 330 nm).

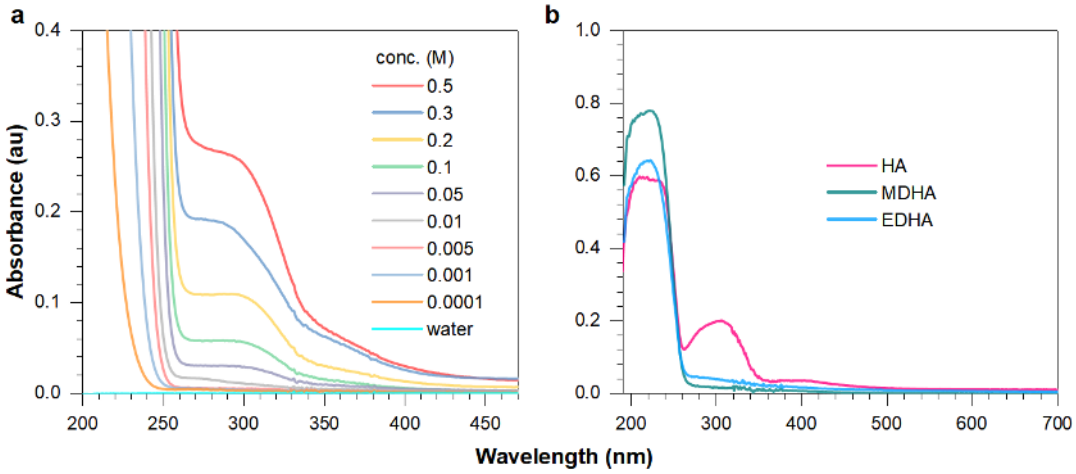

Fig. S13 a,**b**, Absorption of (**a**) varying aqueous HA solutions and (**b**) HA, MDHA and EDHA crystals.

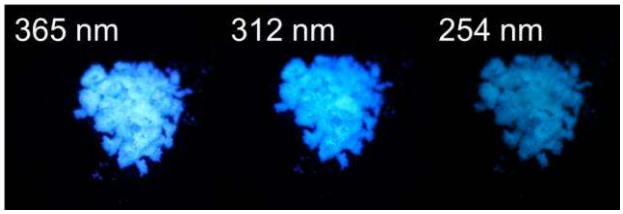

Fig. S14 Photographs of HA crystals taken under different UV lights as indicated.

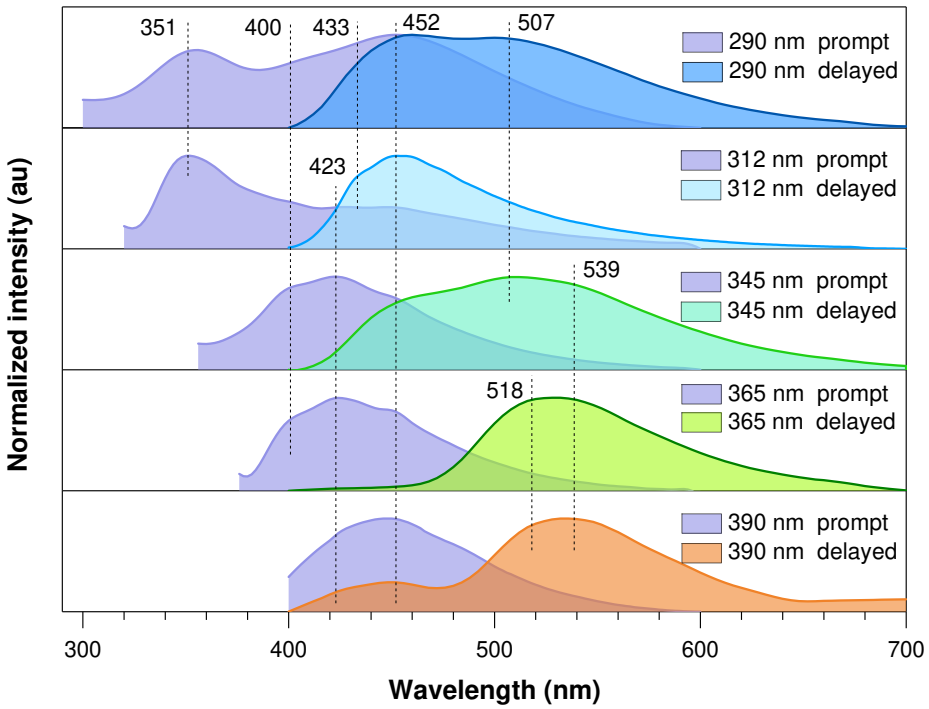

Fig. S15 Normalized prompt and delayed emission spectra of HA crystals under different λ_{ex}s.

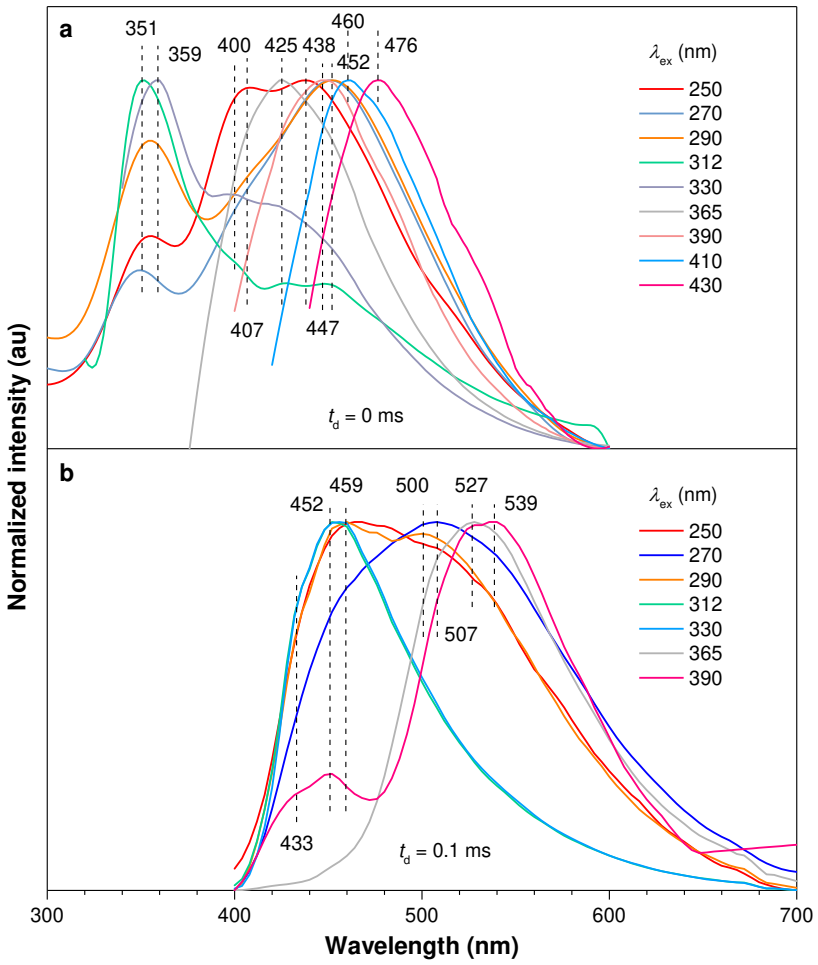

Fig. S16 a,**b**, Normalized (**a**) prompt and (**b**) delayed emission spectra of HA crystals with different λ_{ex}s.

Table S2. p-RTP lifetimes of varying crystals.

Compound	λ_{ex} [nm]	λ_{em} [nm]	$<\tau>_1$ [ms]	$<\tau>_2$ [ms]	$<\tau>_3$ [ms]	B_1 [%]	B_2 [%]	B_3 [%]	χ^2	$<\tau>$ [ms]
HA	312	456	43.8	360.7	1539.5	8.22	25.75	66.03	1.298	1113.0
	365	528	68.1	314.0	1741.6	10.26	15.68	74.06	1.250	1346.0
MDHA	312	450	36.7	312.1	1270.2	6.46	27.39	66.16	1.184	928.2
	365	535	63.8	758.1	--	19.70	80.30	--	1.626	621.3
EDHA	280	510	16.1	128.7	907.5	29.37	27.29	43.34	1.207	433.1
	312	450	100.6	673.0	--	31.70	68.30	--	1.489	491.5
	365	550	17.5	132.8	733.1	14.41	33.43	52.16	1.296	429.3

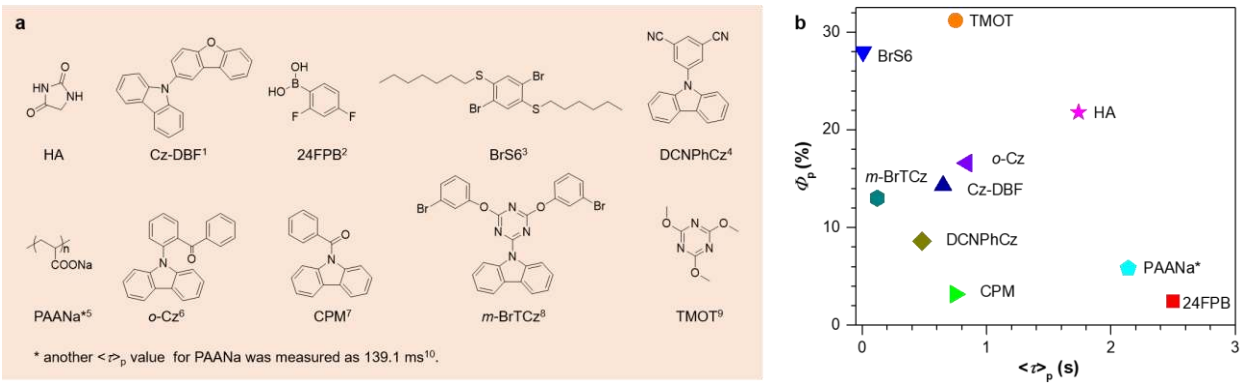

Fig. S17 a, Chemical structures of different luminophores and **b**, their corresponding Φ_p and $<\tau>_p$ values[1-10].

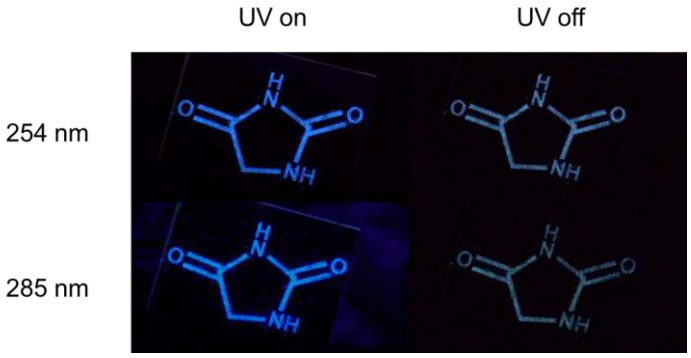

Fig. S18 Photographs of anticounterfeiting patterns based on HA crystals taken under 254 and 285 nm or after ceasing the irradiations.

Table S3. Dynamic photophysical parameters of varying compounds at room temperature.[a)]

Compound	λ_{ex} [nm]	Φ [%]	Φ_f [%]	Φ_p [%]	$<\tau>_p$ [ms]	k_r^p [s^{-1}]	$k_{nr}^p + k_q^p$ [s^{-1}]
HA	312	5.3	2.2	3.1	1539.5	0.02	0.63
	365	87.5	65.7	21.8	1741.6	0.13	0.45
MDHA	312	3.3	2.2	1.1	1270.2	0.01	0.78
	365	17.0	13.4	3.6	758.1	0.05	1.27
EDHA	365	7.3	5.0	2.3	733.1	0.03	1.33

[a)] $<\tau>_p$ is the longest component adopted from the lifetime measurement. $k_r^p = \Phi_p/<\tau>_p$, $k_{nr}^p + k_q^p = (1-\Phi_p)/<\tau>_p$.

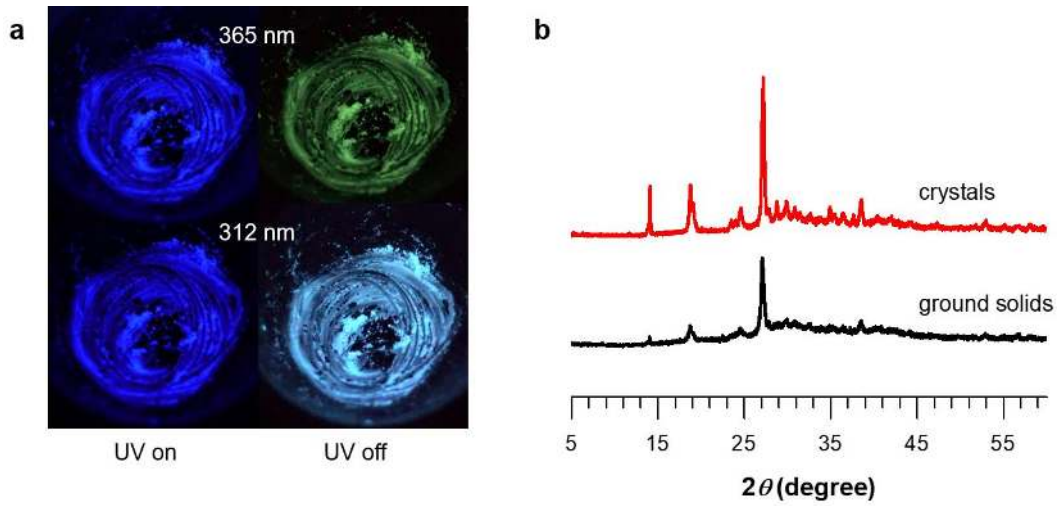

Fig. S19 a, Photographs of ground HA solids taken before and after ceasing different UV excitations. **b**, Power XRD patterns of HA crystals and the ground solids.

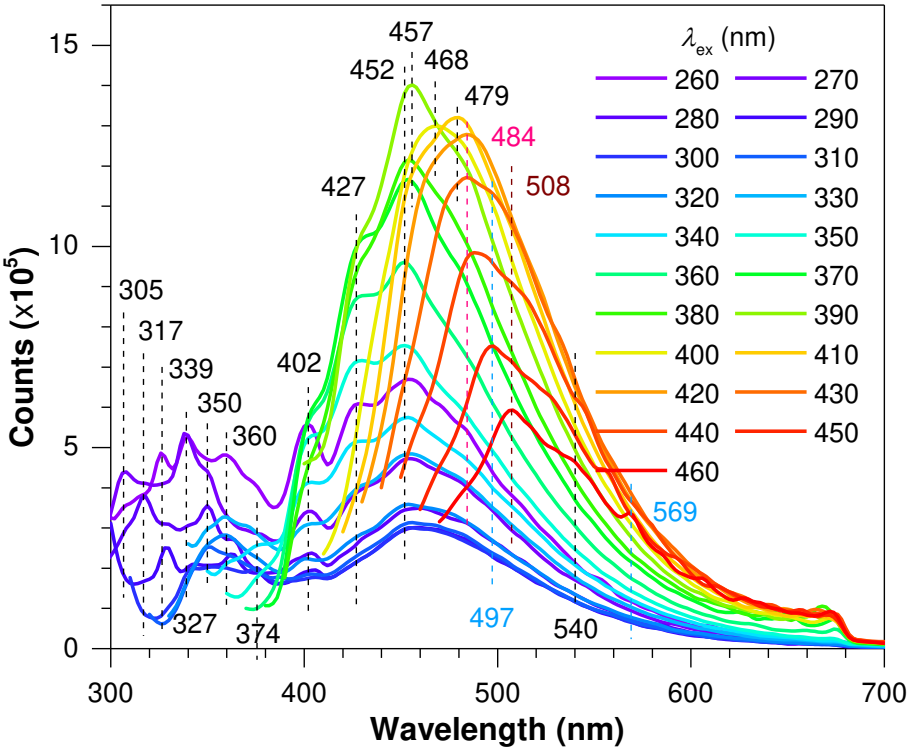

Fig. S20 PL spectra of HA crystals with different λ_{ex}s at 77 K.

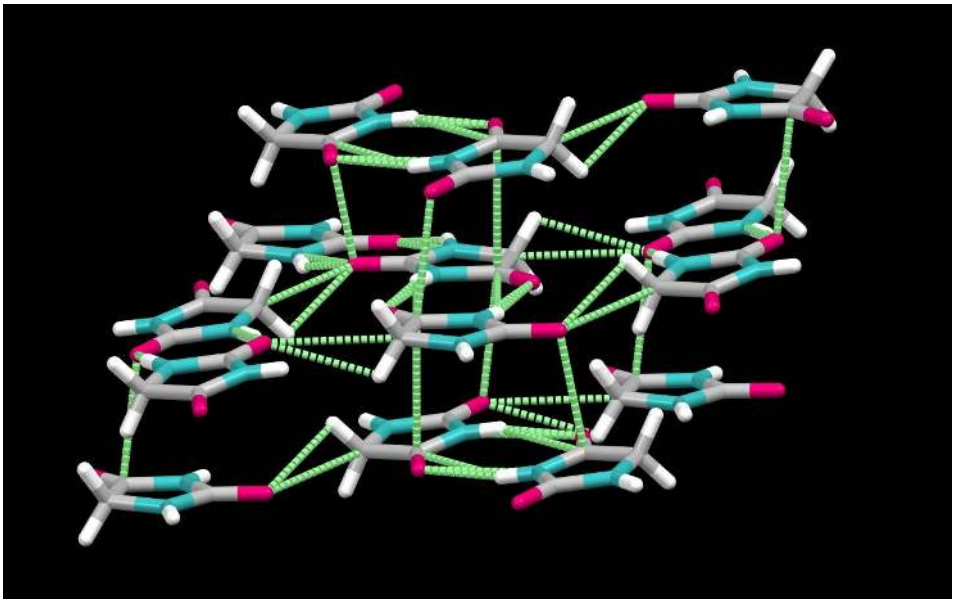

Fig. S21 Fragmental molecular packing and intermolecular interactions of HA crystals.

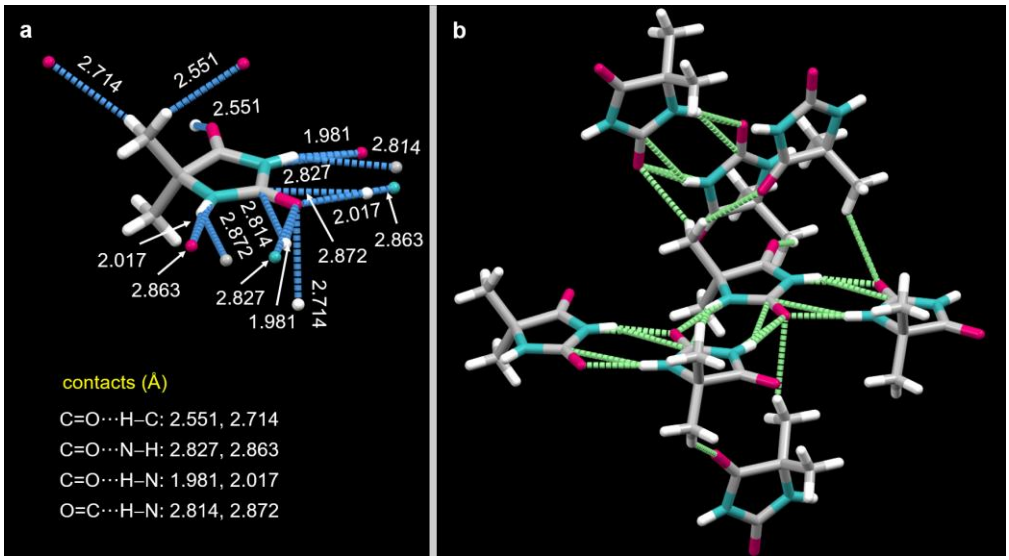

Fig. S22 a, Crystal structure and intermolecular interactions around one molecule in of MHA crystals. **b**, Fragmental molecular packing and intermolecular interactions of MHA crystals.

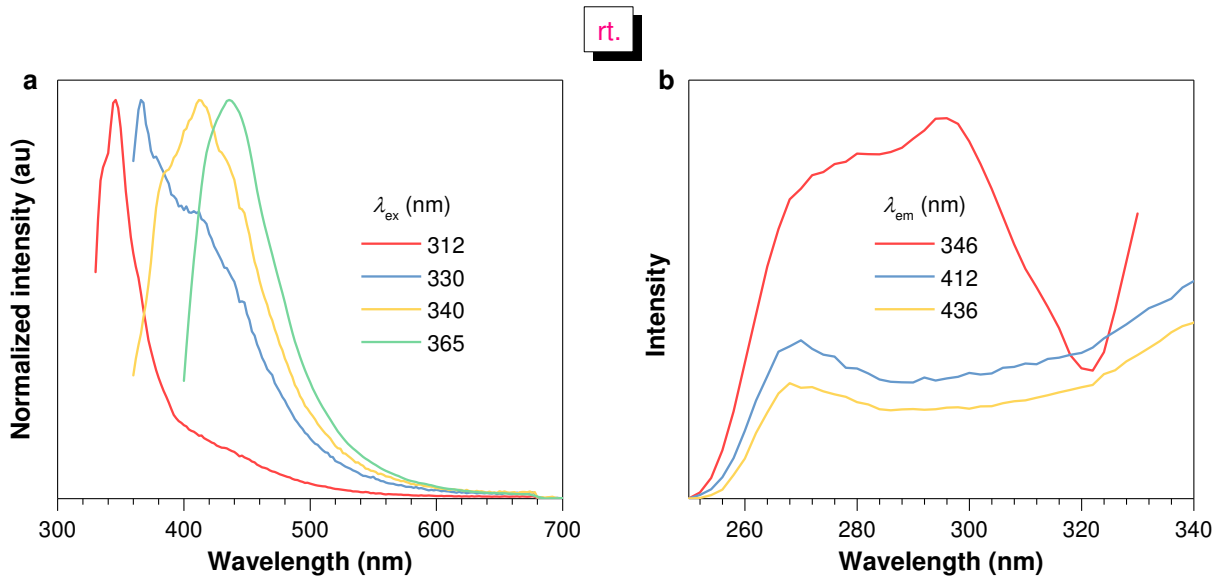

Fig. S23 a, Normalized emission spectra and **b**, excitation spectra of MHA crystals with different (**a**) λ_{ex}s and (**b**) λ_{em}s at room temperature (rt.).

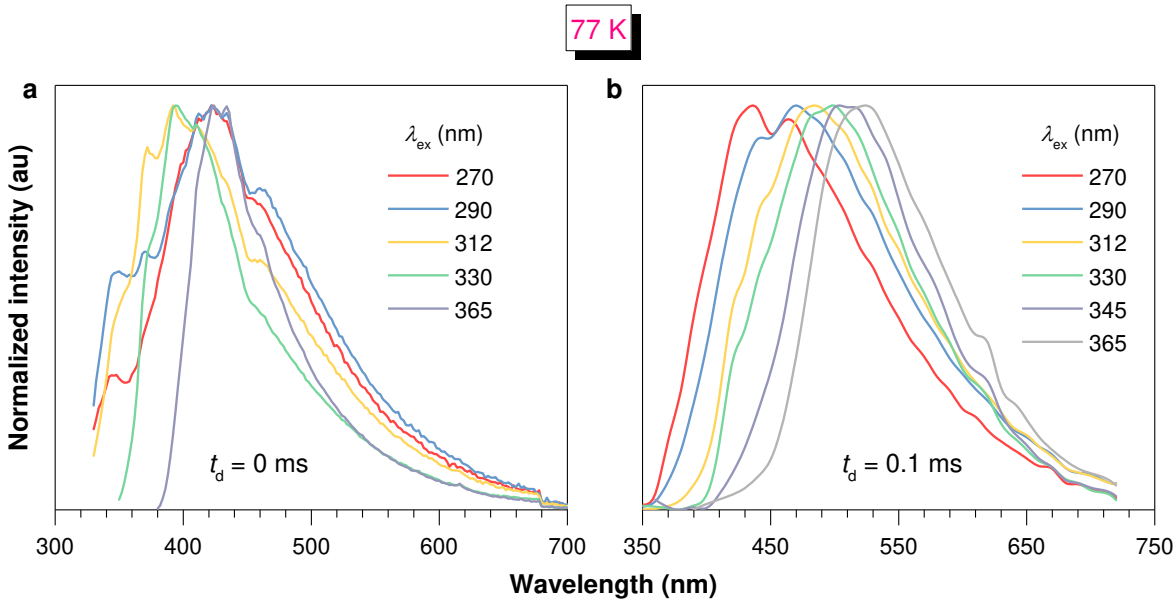

Fig. S24 a,**b**, Normalized (**a**) prompt (t_d = 0 ms) and (**b**) delayed (t_d = 0.1 ms) emission spectra of MHA crystals with different λ_{ex}s at 77 K.

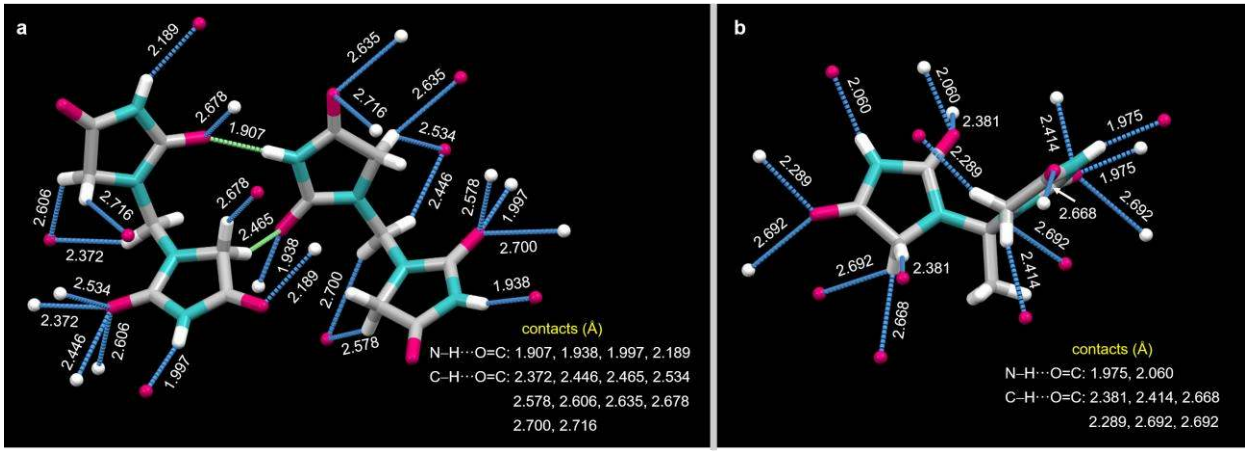

Fig. S25 a,**b**, Single crystal structure of (**a**) MDHA and (**b**) EDHA with denoted N–H···O and C–H···O intermolecular interactions around the molecules.

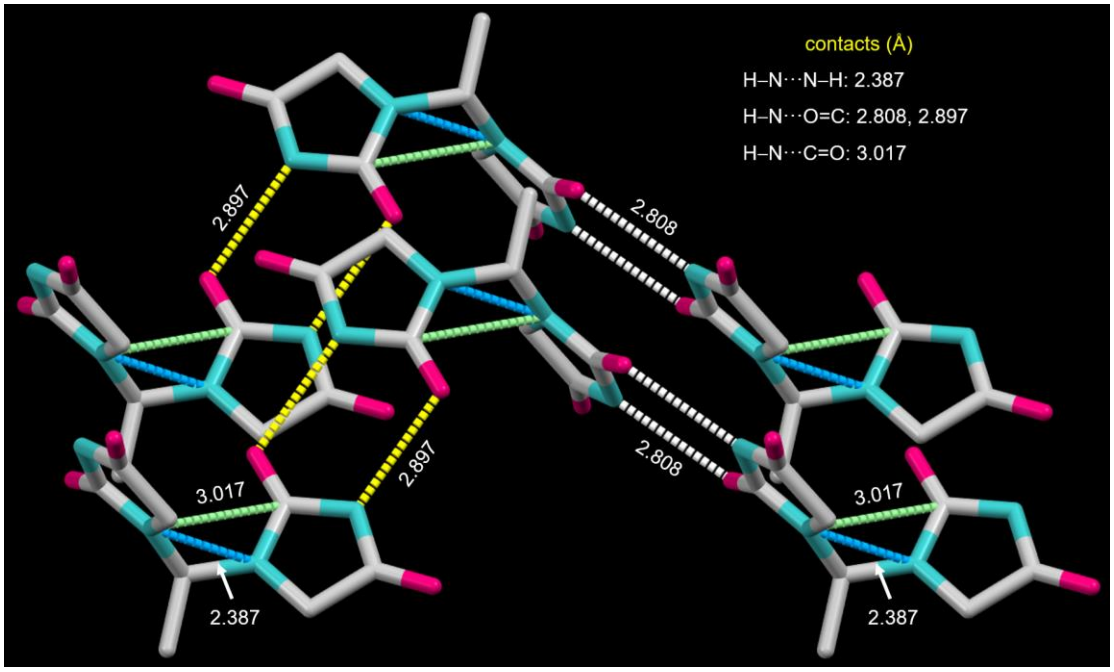

Fig. S26 Fragmental molecular packing of EDHA crystals with 3D through-space conjugation.

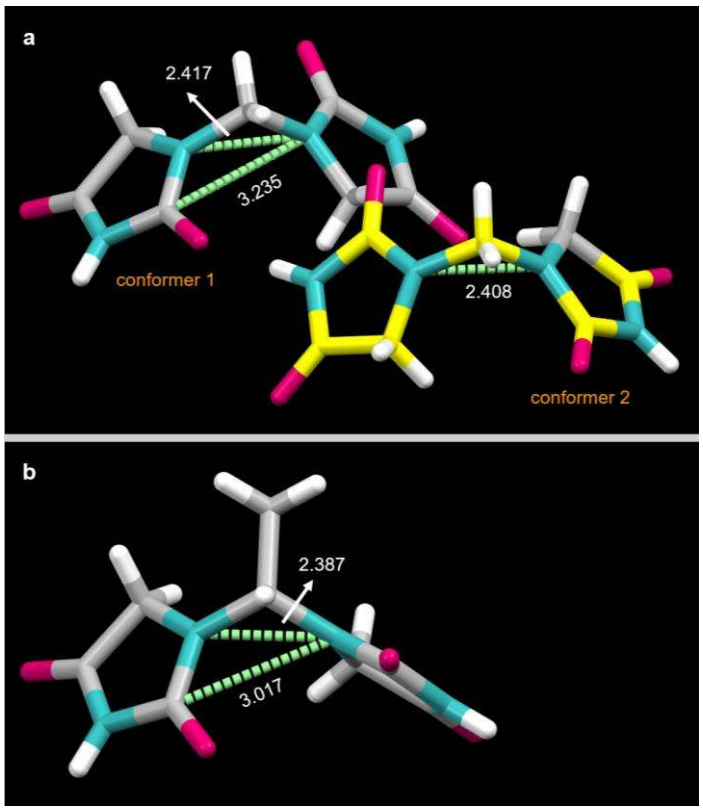

Fig. S27 a,**b**, Crystal structures with denoted intramolecular through-space conjugations for (**a**) MDHA and (**b**) EDHA.

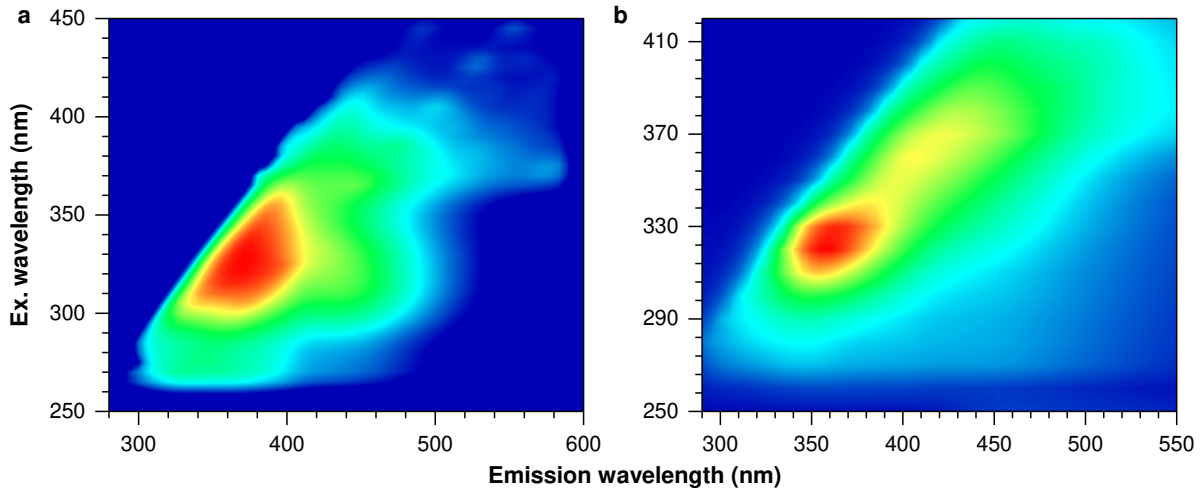

Fig. S28 a,**b**, Excitation-PL mappings of (**a**) MDHA and (**b**) EDHA crystals at room temperature.

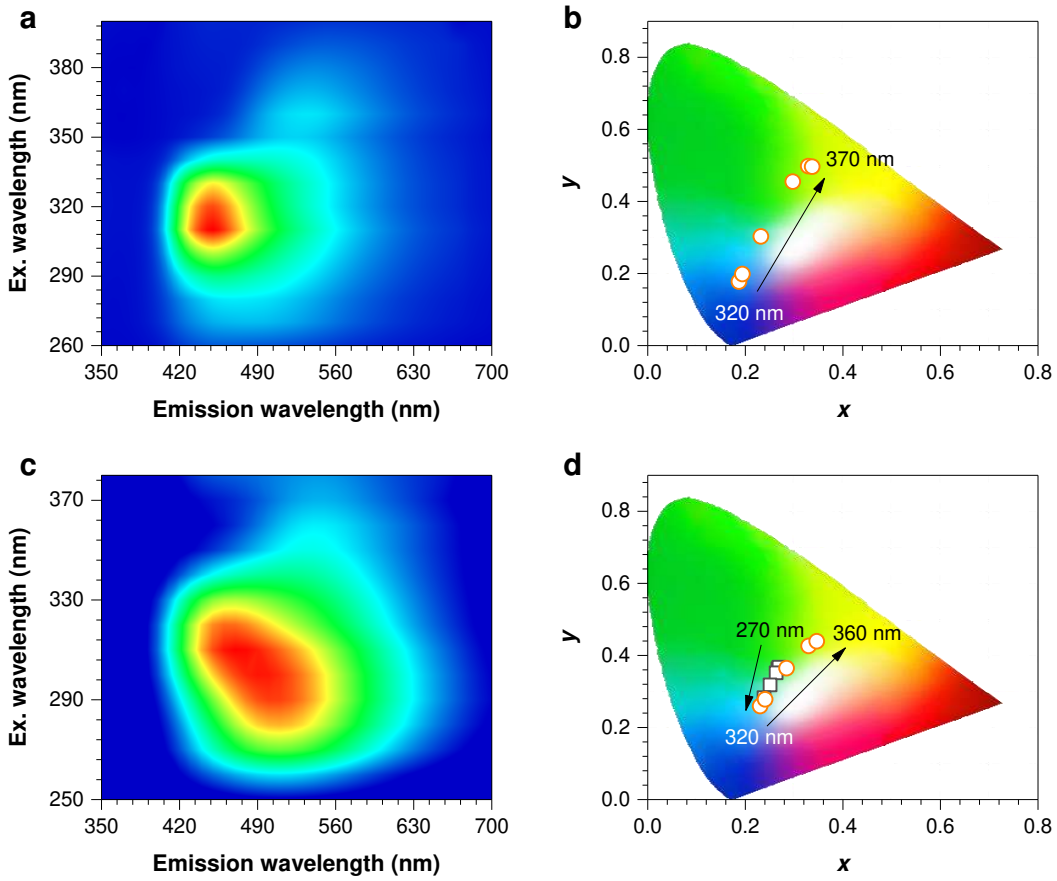

Fig. S29 a,**c**, Excitation-phosphorescence mapping of (**a**) MDHA and (**c**) EDHA crystals (t_d = 0.1 ms). **b**,**d** The CIE coordinate diagrams exhibiting the phosphorescence color variation of (**b**) MDHA and (**d**) EDHA crystals with changing λ_{ex}s.

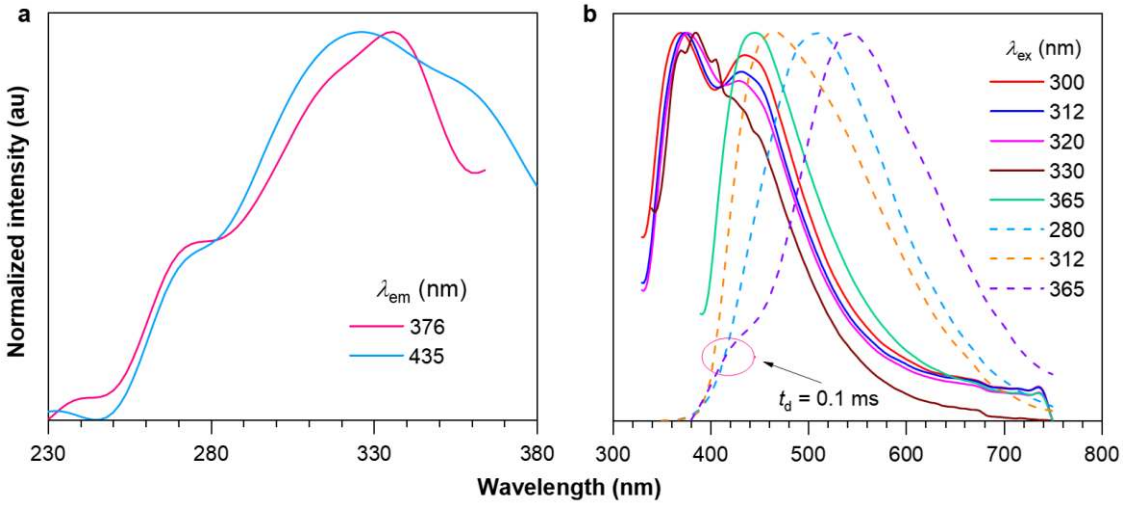

Fig. S30 a, Excitation spectra of EDHA crystals with λ_{em}s of 376 and 435 nm. **b**, Prompt (solid lines) and delayed (dash lines) emission spectra of EDHA crystals upon excitation of different λ_{ex}s.

References

1. Zhao, W.; Cheung, T. S.; Jiang, N.; Huang, W.; Lam, J. W. Y.; Zhang, X.; He, Z.; Tang, B. Z. Boosting the Efficiency of Organic Persistent Room-Temperature Phosphorescence by Intramolecular Triplet-Triplet Energy Transfer. *Nat. Commun.* **2019**, *10*, 1595.
2. Li, M.; Ling, K.; Shi, H.; Gan, N.; Song, L.; Cai, S.; Cheng, Z.; Gu, L.; Wang, X.; Ma, C.; Gu, M.; Wu, Q.; Bian, L.; Liu, M.; An, Z.; Ma, H.; Huang, W. Prolonging Ultralong Organic Phosphorescence Lifetime to 2.5 s through Confining Rotation in Molecular Rotor. *Adv. Opt. Mater.* **2019**, *7*, 1800820.
3. Bolton, O.; Lee, K.; Kim, H. J.; Lin, K. Y.; Kim, J. Activating Efficient Phosphorescence from Purely Organic Materials by Crystal Design. *Nat. Chem.* **2011**, *3*, 205-210.
4. Yuan, J.; Wang, S.; Ji, Y.; Chen, R.; Zhu, Q.; Wang, Y.; Zheng, C.; Tao, Y.; Fan, Q.; Huang, W. Invoking Ultralong Room Temperature Phosphorescence of Purely Organic Compounds through H-Aggregation Engineering. *Mater. Horiz.* **2019**, *6*, 1259-1264.
5. Cai, S.; Ma, H.; Shi, H.; Wang, H.; Wang, X.; Xiao, L.; Ye, W.; Huang, K.; Cao, X.; Gan, N.; Ma, C.; Gu, M.; Song, L.; Xu, H.; Tao, Y.; Zhang, C.; Yao, W.; An, Z.; Huang, W. Enabling Long-Lived Organic Room Temperature Phosphorescence in Polymers by Subunit Interlocking. *Nat. Commun.* **2019**, 10, 4247.
6. Mao, Z.; Yang, Z.; Xu, C.; Xie, Z.; Jiang, L.; Gu, F. L.; Zhao, J.; Zhang, Y.; Aldred, M. P.; Chi, Z. Two-Photon-Excited Ultralong Organic Room Temperature Phosphorescence by Dual-Channel Triplet Harvesting. *Chem. Sci.* **2019**, *10*, 7352-7357.
7. Xie, Y.; Ge, Y.; Peng, Q.; Li, C.; Li, Q.; Li, Z. How the Molecular Packing Affects the Room Temperature Phosphorescence in Pure Organic Compounds: Ingenious Molecular Design, Detailed Crystal Analysis, and Rational Theoretical Calculations. *Adv. Mater.* **2017**, *29*, 1606829.
8. Cai, S.; Shi, H.; Tian, D.; Ma, H.; Cheng, Z.; Wu, Q.; Gu, M.; Huang, L.; An, Z.; Peng, Q.; Huang, W. Enhancing Ultralong Organic Phosphorescence by Effective Π-Type Halogen Bonding. *Adv. Funct. Mater.* **2018**, *28*, 1705045.
9. Gu, L.; Shi, H.; Bian, L.; Gu, M.; Ling, K.; Wang, X.; Ma, H.; Cai, S.; Ning, W.; Fu, L.; Wang, H.; Wang, S.; Gao, Y.; Yao, W.; Huo, F.; Tao, Y.; An, Z.; Liu, X.; Huang, W. Colour-Tunable Ultra-Long Organic Phosphorescence of a Single-Component Molecular Crystal. *Nat. Photonics* **2019**, *13*, 406-411.
10. Zhou, Q.; Wang, Z.; Dou, X.; Wang, Y.; Liu, S.; Zhang, Y.; Yuan, W. Z. Emission Mechanism Understanding and Tunable Persistent Room Temperature Phosphorescence of Amorphous Nonaromatic Polymers. *Mater. Chem. Front.* **2019**, *3*, 257-264.